GEOLOGICAL MAPPING USING REMOTE SENSING TECHNOLOGIES

A THESIS SUBMITTED TO
THE GRADUATE SCHOOL OF NATURAL AND APPLIED SCIENCES
OF
MIDDLE EAST TECHNICAL UNIVERSITY

BY

İNCİ AKKÖK

IN PARTIAL FULFILLMENT OF THE REQUIREMENTS
FOR
THE DEGREE OF MASTER OF SCIENCE
IN
GEOLOGICAL ENGINEERING

MAY 2009

Approval of the thesis:

GEOLOGICAL MAPPING USING REMOTE SENSING TECHNOLOGIES

submitted by **İNCİ AKKÖK** in partial fulfillment of the requirements for the degree of **Master of Science in Geological Engineering Department, Middle East Technical University** by,

Prof. Dr. Canan Özgen _____
Dean, Graduate School of **Natural and Applied Sciences**

Prof. Dr. M. Zeki Çamur _____
Head of Department, **Geological Engineering**

Assoc. Prof. Dr. M. Lütfi Süzen _____
Supervisor, **Geological Engineering Dept., METU**

Assoc. Prof. Dr. Nuretdin Kaymakçı _____
Co-Supervisor, **Geological Engineering Dept., METU**

Examining Committee Members:

Prof. Dr. Vedat Doyuran _____
Geological Engineering Dept., METU

Prof. Dr. Nurkan Karahanoğlu _____
Geological Engineering Dept., METU

Assoc. Prof. Dr. M. Lütfi Süzen _____
Geological Engineering Dept., METU

Assoc. Prof. Dr. Bora Rojay _____
Geological Engineering Dept., METU

Dr. Arda Arcasoy _____
Arcasoy Consulting and Eng. Co.

I hereby declare that all information in this document has been obtained and presented in accordance with academic rules and ethical conduct. I also declare that, as required by these rules and conduct, I have fully cited and referenced all material and results that are not original to this work.

Name, Last Name: İnci AKKÖK

Signature:

ABSTRACT

GEOLOGICAL MAPPING USING REMOTE SENSING TECHNOLOGIES

Akkök, İnci

M.Sc., Department of Geological Engineering
Supervisor : Assoc. Prof. Dr. M. Lütfi Süzen
Co-Supervisor: Assoc. Prof. Dr. Nuretdin Kaymakçı

May 2009

In an area of interest- Sivas Basin, Turkey- where most of the units are sedimentary and show similar spectral characteristics, spectral settings of ASTER sensor may not be enough by itself. Therefore, considering other aspects, such as morphological variables, is reasonable in addition to spectral classifiers. The main objective of this study is to test usefulness of integration of spectral analysis and morphological information for geological mapping. Remotely sensed imagery obtained from ASTER sensor is used to classify different lithological units while DEM is used to characterize landforms related to these lithological units.

Maximum Likelihood Classification (MLC) is used to integrate data streaming from different sources. The methodology involves integrating the surface properties of the classified geological units in addition to the spectral reflectances. Seven different classification trials were conducted: : 1. MLC using only nine ASTER bands, 2. MLC using ASTER bands and DEM, 3. MLC using ASTER bands and slope, 4. MLC using ASTER bands and plan curvature, 5. MLC using ASTER bands and profile curvature, 6. MLC using ASTER bands and drainage density and finally 7. MLC using ASTER bands and all ancillary data.

The results revealed that integrating topographical parameters aid in improvement of classification where spectral information is not sufficient to discriminate between classes of interest. An increase of more than 5% is observed in overall accuracy for the all ancillary data integration case. Moreover more than 10% improvement for most of the classes was identified. However from the results it is evident that the areal extent of the classified units causes constraints on application of the methodology.

Keywords: Remote Sensing, ASTER, lithological mapping, ancillary data, Sivas basin

ÖZ

UZAKTAN ALGILAMA TEKNOLOJİLERİ KULLANILARAK JEOLOJİK HARİTALAMA

Akkök, İnci

Yüksek Lisans, Jeoloji Mühendisliği Bölümü
Tez Yöneticisi : Doç. Dr. M.Lütfi Süzen
Ortak Tez Yöneticisi: Doç. Dr. Nuretdin Kaymakçı

Mayıs 2009

Sivas havzasında yer alan çalışma sahasında olduğu gibi ,sahanın çoğunluğunun sedimanter kayaçlardan oluştuğu ve benzer spektral özellikler gösterdiği bir durumda, yalnızca ASTER sensörü yeterli olmayabilir. Bu nedenle spektral sınıflandırmaya ek olarak morfolojik parametrelerin de kullanılması öngörülebilir. Bu araştırmanın amacı, farklı kayaç topluluklarının daha hassas haritalanabilmesi için spektral özelliklerin yanısıra yüzey parametrelerinin kullanımının etkinliğini test etmektir. ASTER görüntüleri farklı kayaçlar için sınıflandırılmış ve SYM kullanılarak yüzey özelliklerinden yararlanılmıştır.

Farklı kaynaklardan gelen verilerin birarada değerlendirilmesinde Maksimum Benzerlik (MB) algoritması kullanılmıştır. Metodoloji sınıflanan jeolojik birimlerin spektral özelliklerinin kullanılmasının yanı sıra, yüzey özelliklerinin de birlikte hesaba katılmasını içermektedir.. Öncelikle yalnızca dokuz ASTER bandı ile MB sınıflandırması, diğer altı sınıflandırma da dokuz ASTER bandı ve yardımcı verilerin ayrı ayrı MB ile sınıflandırması olacak şekilde yedi farklı sınıflandırma yapılmıştır.

Bunların sonucunda, değerlendirilen sınıfların birbirlerinden ayrılmasında spektral özelliklerinin yeterli olmadığı durumlarda yüzey parametrelerinin sınıflandırmanın doğruluğunun artırılmasında faydalı olduğunu göstermiştir. Tüm yardımcı verinin birlikte değerlendirildiği sınıflandırmada, genel doğruluğun %5'den fazla arttığı belirlenmiştir. Buna ek olarak, sınıfların çoğunluğunun doğruluğunda ayrı ayrı %10'dan fazla artış gözlemlenmiştir. Ancak sonuçlar sınıflanan birimlerin kapladığı alanların metodolojinin uygulanması açısından sıkıntı yaratabildiğini ortaya çıkarmıştır.

Anahtar kelimeler: Uzaktan Algılama, ASTER, litolojik haritalama, yardımcı veri, Sivas havzası

To my parents

ACKNOWLEDGEMENTS

I would like to forward my great thanks to my supervisor Assoc. Prof. Dr. M. Lütfi Süzen for his help, contribution and support. Without his advice, guidance and suggestions this would not be possible.

Special thanks to my co-supervisor Assoc. Prof. Dr. Nuretdin Kaymakçı for his support and help during each step of my graduate education.

I am thankful to Assoc. Prof. Dr. Bora Rojay for his constant encouragement since the beginning of my undergraduate education in the department and for providing me the opportunity to extend my education beyond the borders.

I would like to thank Geological Engineering Department and especially RS-GIS Lab. members for their contribution throughout my graduate work.

Many thanks to my classmates for their company and especially Ceren for sharing the thesis period, cheerful times and difficulties with me.

I would like to thank my parents for their lifetime support and belief in me.

TABLE OF CONTENTS

LIST OF TABLES

TABLES

LIST OF FIGURES

FIGURES

CHAPTER 1

INTRODUCTION

1.1 Purpose and Scope

Application of Remote Sensing (RS) for geological mapping and/or exploration has rapidly increased during the last decade. Availability and accessibility of satellite images with high spatial and spectral resolution, together with implementation of Geographical Information Systems (GIS) tools has improved the mapping process which is beneficiary for any kind of study. Just like the 60 km swath width of ASTER (Advanced Spaceborne Thermal Emission and Reflection Radiometer) covers an area of 3600 km^2 with 14 different bands ranging between 0.52-11.25 μms, including one back-looking band to produce a Digital Elevation Model of the observed terrain could easily be ordered for a few hundred US dollars from the World Wide Web.

Although the accessibility and availability of satellite images are increased drastically, the observed target is still the same with well known problems like presence of spectral mixtures, uneven illumination conditions, inhomogeneous mapping units like geological formations, etc. Furthermore the increases in spectral, spatial and radiometric resolutions still might not be adequate enough to discriminate surface materials where there are spectrally similar units consisted of similar lithologies. However, the integration of spectral data with additional ancillary data can be considered, namely the topographic expression i.e. properties

such as topographic parameters of various lithologies, to further discriminate the mapping units.

The integration of GIS in spectral classification have been studied elaborately by Hutchinson (1982), Strahler (1980) especially in landcover studies, where the spectral mixtures are generally dominated by homogenous pixels and homogenous mapping units. Whereas especially in geological mapping, degree of homogenization of one formation is not limited to only one lithology, many lithologies could form up in one formation resulting in heterogeneous pixels with definition limited homogenous mapping units.

The aim of this thesis is to evaluate the possible contributions of ancillary topographic data in image classification beyond the scope of lithological mapping of spectrally similar surface units.

1.2 Objectives

The main objective of this study is to test usefulness of integration of spectral analysis and terrain information for geological mapping. In order to support this main objective, the research specifically aims to:

1. Improve the mapping accuracy of spectrally similar units using integration of terrain parameters.
2. Determine which terrain attributes obtained from Digital Elevation Model (DEM) can be used in extraction of geologic information
3. Identify which lithologies can be better differentiated on the basis of terrain parameters

1.3 Research Methodology and Data

The methodology consists of integrating information streaming from different sources. Spatial, as well as the spectral information is taken into account, aiming at improving the image classification results. For image processing and analysis, Microimages TNT software was employed.

Available data consist of:
- ASTER imagery
- DEM derived from digitization of 1/25 000 topographic map contours
- 1/100 000 geologic maps (F25 and F26 sheets)
- 1/ 25 000 topographic maps (i39d2-d3, i39c1-c2-c3-c4, i40d1-d4)

ASTER data is used for spectral mapping for depiction of lithologies in the study. A subset including the major rock units was selected from the snow and cloud free original image. DEM derived from digitization of 1/25 000 topographic maps is resampled to the same resolution, projection, and datum. DEM derived from contours is utilized for extraction of terrain parameters used as additional means of classifying the lithologies in addition to spectral properties. Coordinate system is UTM Zone 37 and datum is European 1950-Mean.

Study area is located in southeast Sivas and South of Zara (Figure 1.1). The area is part of Sivas Tertiary Basin; which is a basin developed mainly on the Neo-Tethyan ophiolitic suture separating the Tauride Platform in the south from the Pontides in the north (Yılmaz and Yılmaz, 2006), and is one of the important basins in Central Anatolia. The study area covers an area of approximately 888 km^2 and is located between Northing coordinates of 4373258 and 4399254 and Easting coordinates of 382249 and 424951. Most of the rock units that crop out in the study area are sedimentary and spectrally similar. However there are noteable differences in the surface morphology which makes this site ideal for the proposed study. The detailed geology of the area is given in Chapter 2.

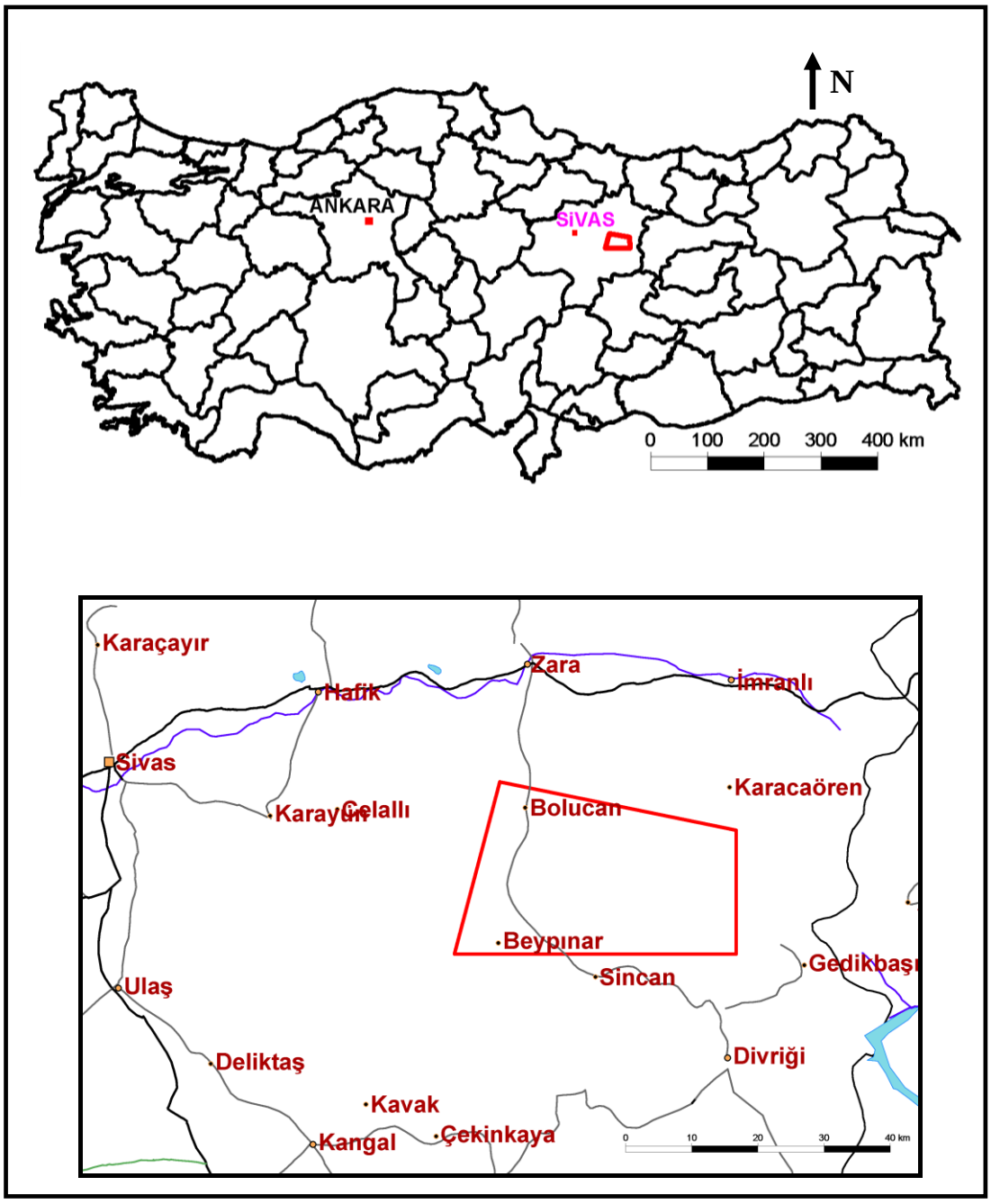

Figure 1.1: Location map of the study area

CHAPTER 2

GEOLOGY OF THE AREA

The Sivas Basin is a complex collage of Eocene and younger rocks located within the wedge-shaped eastern margin of the Anatolian Block between the dextral North Anatolian Fault Zone and the sinistral East Anatolian Fault Zone (Figure 2.1). The basin is situated at the eastern part of the central Anatolia where three main tectonic units, converge to each other, namely along Kelkit Valley- the Pontides, along the west; the Kırşehir block and Tauride platform in the south along Tecer Mountains (Ocakoğlu, 1999).

The basin has been subject to ongoing deformation by movement of the Arabian Block into Eurasia and associated sideways expulsion of the Anatolian Block. Post-collisional deformation since mid-Miocene times has been dominated by N-S to NW-SE compression expressed by thrusting and strike-slip faulting (Gürsoy et al. 1997)

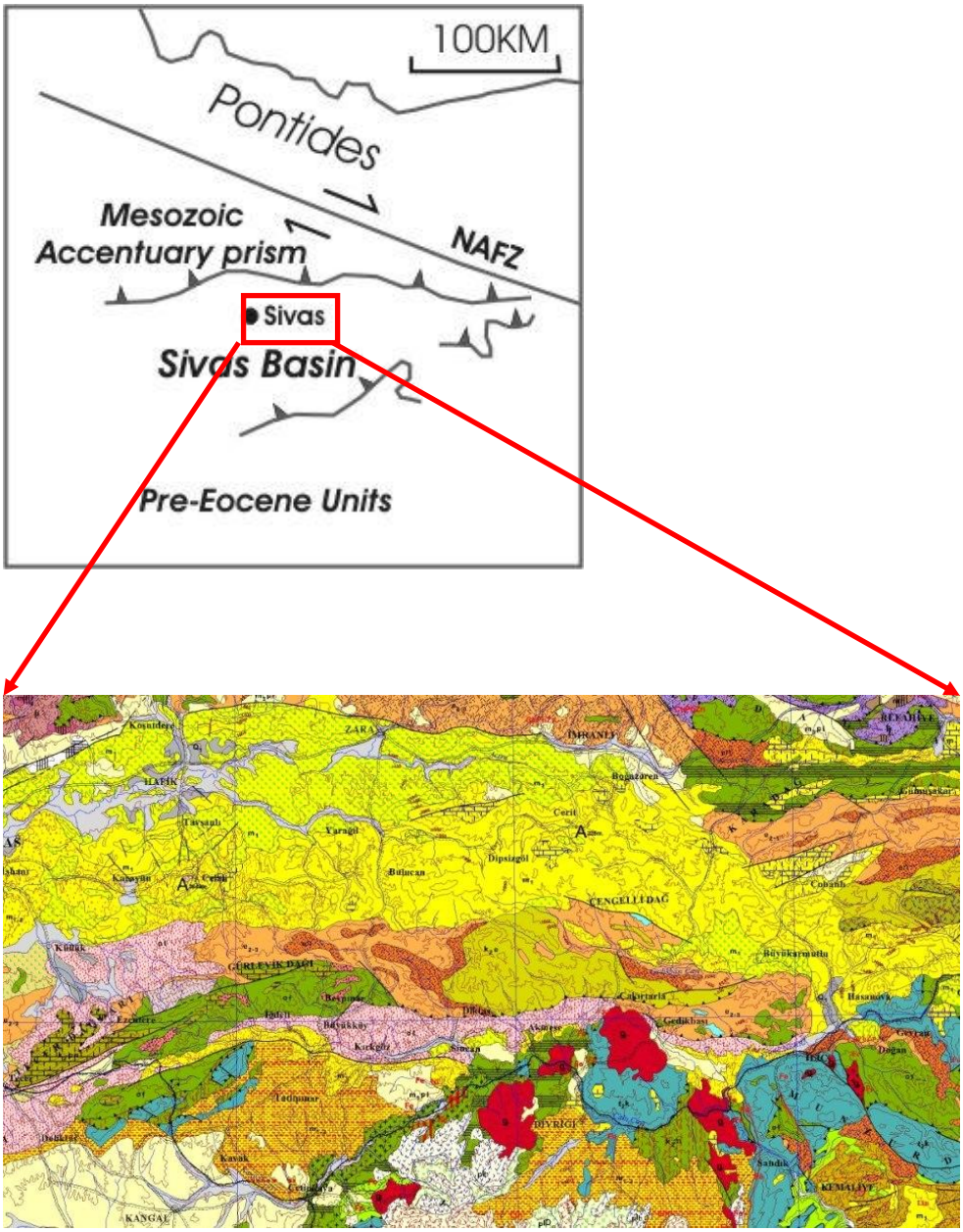

Figure 2. 2: Regional geological map (MTA 1/ 500.000 scale map)

2.1 Previous Studies

The study area is located in the Sivas Basin. The basin extends approximately 60 km long and 30 km wide and covers a considerable large area with numerous geological features and economical aspects which can be of interest for many researchers and the industry. Therefore, large numbers of studies have been performed related to different geological features and different locations in the basin. Literature related with the scope of this study, can be grouped under the attempts made in order to investigate the stratigraphy and tectonics of the region.

Among these, Kurtman (1961) is the first published work in literature. He has identified the rock units which crop-out in the region and studied the stratigraphy and structure. Accordingly, Paleozoic- Quaternary units crop-out in the region and the region has been subjected to folding; in the end of Paleozoic, at Late Cretaceous, at Late Eocene and Late Miocene.

Artan and Sestini (1971) prepared geological map of Sivas-Zara-Beypınarı region and studied petrology of ophiolitic rocks and flysch, and genesis of asbestos found in the region. They assumed a Late Cretaceous emplacement age for the ophiolitic rocks. They proposed that the general sense of tectonic movements are from South to North and the serpentinites which are the main rock of the ophiolitic complex have been thrusted over Lower Paleocene limestones and Eocene flysch. Folding and thrust movements were generated in the Late Eocene and post-geosynclinal evaporites, limestone and sandstones were deposited afterwards.

Kurtman (1973) investigated the Sivas- Hafik-Zara and İmranli region at 1/100000 scale and concentrated on the geological and tectonic setting and the problems faced during previous studies. This is the first study in nomenclature of Tertiary stratigraphy and age determinations of the formations are made.

He divides the region into three tectonic zones: 1. Sakardağ-Kösedağ Uplift, 2. Hafik- Zara-İmranli depression and 3. Tecer-Gürlevik Uplift. In addition detailed structural studies related to the fold axes and joints for each formation are carried out.

Aktimur et al. (1990) covered the area from Sivas to Erzincan and aimed to exhibit basic geological characteristics of the Tertiary basin. The study is mostly compiled from previous works of the first author; including the 1/100 000 scale geological maps (F24, F25 and F26 sheets) published by MTA and include the new nomenclature proposed for the units. They suggested that the ophiolitic complex has emplaced in the Late Cretaceous and moved several times until the end of Early Miocene. It is stated that Maastrichtien-Paleocene-Eocene clastics unconformably overlying the ophiolitic complex are vertically transitional and Oligo-Miocene and Early-Mid Miocene clastics are both laterally and vertically transitional. The region has become a continental setting by Late Miocene. In the Neotectonic period, strike-slip faults are developed in the region.

Cater et al. (1991) studied the Tertiary evolution of the central and western parts of the basin and suggested the ophiolitic mélange was emplaced prior to Eocene and region filled rapidly with gravity-flow deposits. Infilling and shallowing of basin recorded towards the end of Eocene is a marker of tectonic compression. Following the thrust reactivation, in other words regional tectonic shortening at the end of Oligocene, slices of ophiolite and Eocene sediments were moved northward. It is suggested that the basin was floored by a thrust sheet formed during Oligocene compression and the floor was divided into N-S elongated fault-bounded blocks. This lead to differential subsidence of the blocks during Miocene and formation of growth folds. Another period of tectonic compression is specified and related to the initiation of Northern Boundary Fault of the basin during the Miocene. It is proposed that there has been at least two phases of uplift during Pliocene.

Koşun and Çiner (2002) mapped and studied the Miocene stratigraphy of the south of Zara and proposed a new formation and member nomenclature for the sequences. Hafik gypsum formation was assumed to be Oligocene-Early Miocene.

Yılmaz and Yılmaz (2006) interpreted the basin as a post-collusional; intracontinental basin that developed mainly after closure of the northern branch of Neo-Tethys. They suggested that the basin was formed on a basement consisting of ophiolitic units of northern branch of Neo-Tethys obducted onto the Tauride Platform and its metamorphic equivalents (Akdağmadeni-Kırşehir metamorphics).

2.2 Stratigraphy

In the study area Cretaceous basement ophiolites and Upper Cretaceous, Eocene, Oligocene, Miocene, Pliocene and Quaternary rock formations are observed and a generalized stratigraphic columnar section for the basin is given in Figure 2.2.

Lithologies have been previously mapped by Kurtman (1973), Aktimur (1988) and Aktimur and Tütüncü (1988) (Figure 2.3).

The rock sequence in the investigated area consists of:

1. Cretaceous ophiolitic basement
2. Upper Cretaceous-Paleocene carbonates and flysch
3. Eocene sedimentary rocks of turbiditic flysch character with tuffite intercalations
4. Oligocene evaporites, limestones and clastics
5. Miocene shallow marine and fluvial deposits;
6. Pliocene fluvial deposits; and
7. Quaternary fluvial deposits

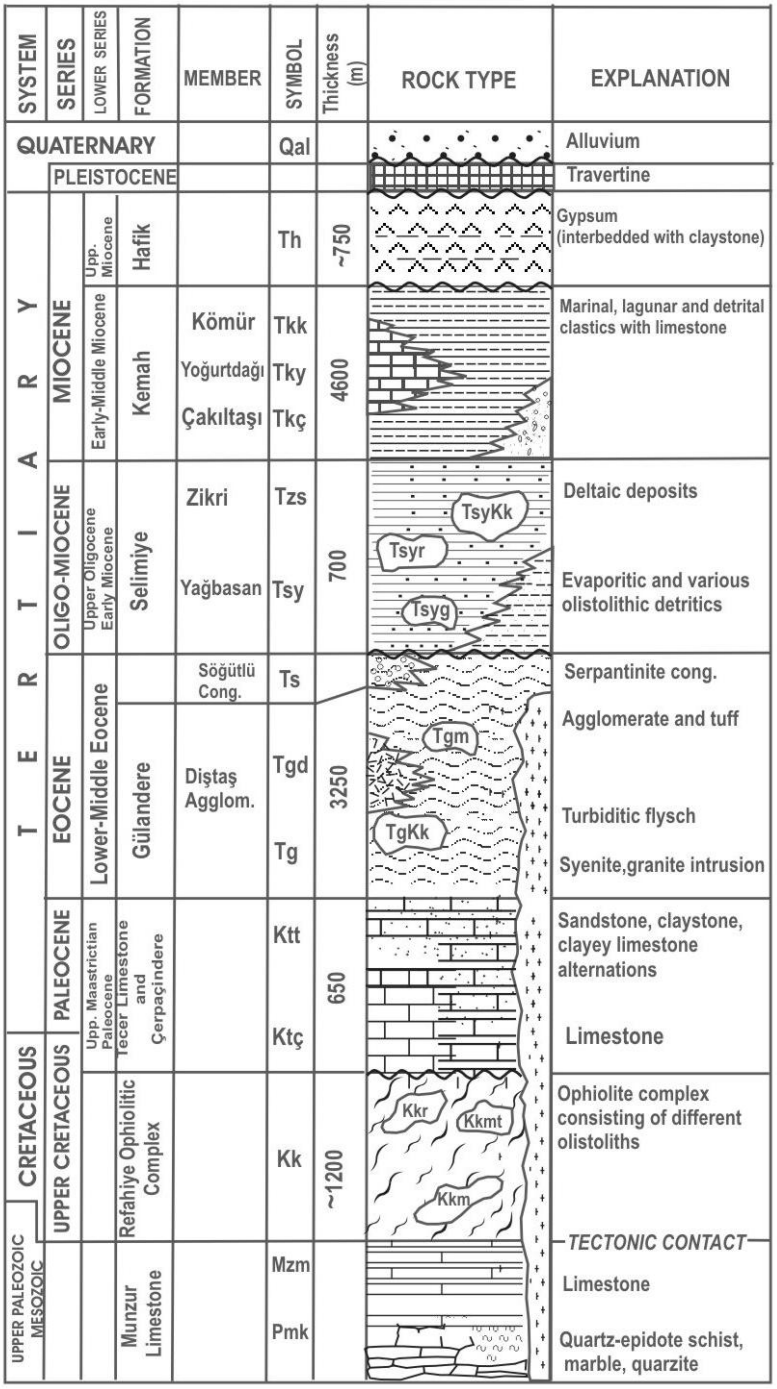

Figure 2. 2: Generalized stratigraphic section of Tertiary basin between Sivas-Erzincan (modified from Aktimur et. al., 1990)

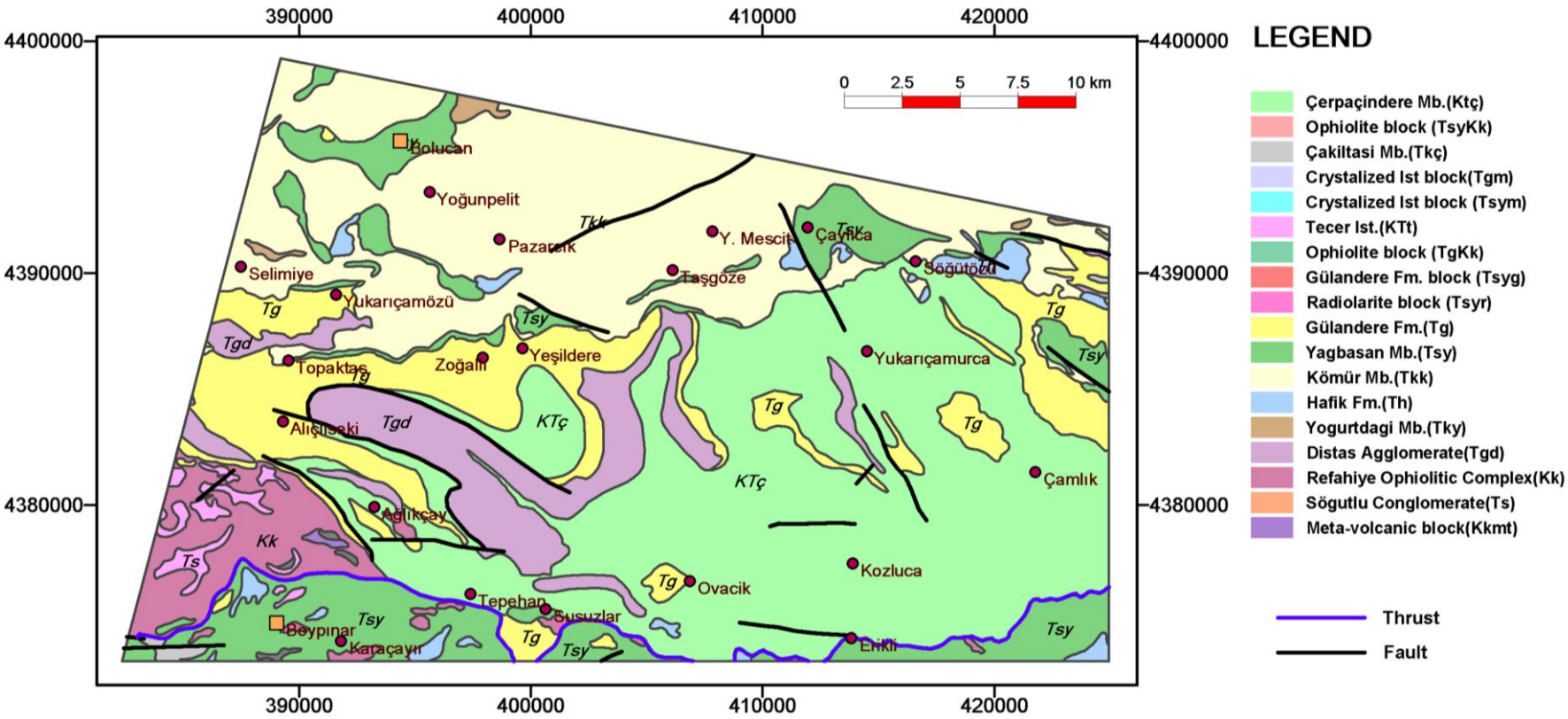

Figure 2. 3: Geological map of the study area (modified from F25 and F26 sheets, MTA, 1988)

For the study area it is implied that, Refahiye ophiolitic complex are overlain by Upper Maastrichtian - Paleocene Tecer limestone and Çerpaçindere formation. This formation passes to Eocene Gülandere formation with flysch character. Oligo-Miocene and Miocene marine, lagunar and continental detritics with evaporites and carbonates, are deposited unconformably on all these units. Plio-Quatemary is represented by continental deposits and by volcanics (Aktimur et al. 1990). The explanations of the units are taken from Aktimur et al. (1990) and from the texts in 1/ 100 000 geological maps, F25 and F26 sheets, published by MTA (1988). The following paragraphs briefly describe the formations in chronological order.

2.2.1. Cretaceous

Refahiye ophiolitic complex

The oldest rock unit which crop out in the area is the Refahiye ophiolitic complex. Refahiye ophiolitic complex generally has mixtures of dark green, dark brown, dark gray hard, blocky disintegrated dunite, peridotite, serpentinite, amphibolite, gabbro.

2.2.2. Upper Cretaceous

Tecer limestone

Tecer limestone is the oldest sedimentary formation present in the study area. It is deposited unconformably on the Refahiye ophiolites. They consist of gray-dark grey, black, medium to thick bedded, jointed, micritic textured limestones.

2.2.3. Upper Cretaceous- Paleocene

Çerpaçindere formation

The unit is examined in two members: Çerpaçin member having successions of conglomerate, sandstone, sandy limestone, clayey limestone and Karadağ basalt having andesite, basalt, tuff and agglomerates. Only Çerpaçin member is present in the study area.

Çerpaçin member. - The unit comprising successions of sandstone, conglomerate, claystone, clayey limestone, sandy limestone and tuff is generally gray, green, reddish coloured, calcite veined and sandstone is cross-bedded. In upper parts, Çerpaçin member passes gradually into Eocene Gülandere formation.

2.2.4. Eocene

Eocene units unconformably overlie the older formations. Units start with conglomerate layers and develop into flysch character both vertically and laterally towards the center of the basin. In addition, especially in the Middle Eocene flysch layers, andesite, tuffite and volcanic breccia levels exist in the sequence (Kurtman 1973, Artan and Sestini 1971).

Gülandere formation

Gülandere formation is described by Kurtman (1973) and Aktimur (1988). The formation generally having turbiditic flysch character consists of successions of sandstone, claystone, conglomerate, siltstone, tuffs and agglomerates (Dişta agglomerate). Unit includes andesitic and basaltic lavas with olistostromal blocks of Refahiye ophiolitic complex. The unit is multicoloured (gray, brown, red, green, blue), thin, medium to thick bedded, folded, faulted and jointed.

The Gülandere formation gradually grades into the Çerpaçindere formation, which was deposited in deep sea environment. Horizontal movements causing repetitions in the sequence and the andesitic basaltic volcanism, is contemporaneous with deposition. These horizontal movements also dragged large units (olistoliths) from Refahiye ophiolitic complex to the depositional basin. This formation is widespread in the Sivas Basin and at some places reaches up to 4500 m thickness.

Söğütlü conglomerate

It was defined as Söğütlü complex by Arpat (1964). However due to the unit having only conglomerate, it was named as Söğütlü conglomerate by Aktimur (1988). It is blackish green, reddish and thickly bedded conglomerates of serpentinites.

2.2.5. Oligocene

Selimiye formation

This formation, which is composed of gypsum, sandstone, marl and dolomitized limestones, overlies unconformably Gülandere formation and gradually grades into Kemah formation (Kurtman, 1973). This formation is divided into Yağbasan and Zikri members (Aktimur, 1988). In the study area only Yağbasan member is present.

Yağbasan member. - The member is represented by successions of sandstone, claystone, mudstone, gypsum and conglomerate. It is multicoloured (red, gray, greenish, white) thin to medium bedded, jointed and in places overturned and folded Unit begins with conglomerate in some places and with gypsum in others. The member deposited in shallow sea, lagoon and continental environs, varies in thickness.

2.2.6. Miocene

Kemah formation

The unit was described by Özgül (1981) and generally consists of conglomerates siltstone, sandstone and limestones. The formation has some blocky levels, as a result of overthrusting by synsedimentary bending.

Kemah formation was observed as grading to Selimiye formation and was unconformably overlain by Hafik formation. Kemah formation was divided into the members of Çakıltaşı, Kömür and Yoğurtdağı (Aktimur, 1988).

The Çakıltaşı member. - The member generally consists of reddish, green, in places grayish coloured, medium to thick bedded, argillaceous and carbonate cemented, well sorted conglomerate and sandstones grades vertically and horizontally to the Kömür member.

The Kömür member. - The unit is formed by successions of multicoloured (red, yellow, white, gray, green) thin to thick bedded sandstone, claystone, mudstone, clayey limestone and siltstone. The unit is folded, jointed, over turned folded in places, friable and altered.

The Yoğurdağı member- The unit, formed by limestones, is white colored, medium to thick bedded, calcite veined, jointed and conchoidal fractured. The Yoğurtdağı member is deposited in shallow marine environment and grades horizontally into Kömür member.

The Hafik formation

The unit dominantly consists of white coloured gypsum and successions of multicoloured (red, dark red, green, blue) claystone and sandstone.

2.2.7. Pliocene

Pliocene deposits are composed of claystone and limestone interbedded with conglomerate and sandstone (Altunsoy and Özçelik, 1998).

CHAPTER 3

BACKGROUND INFORMATION ON REMOTE SENSING, IMAGE CLASSIFICATION AND TERRAIN ANALYSIS

Geological mapping is one of the most time and effort taking activities of geologists and involves the identification of landforms, rock types and rock structure and the portrayal of geologic units and structure on a map or other display in their correct spatial relationship with one another. However, in classical optical remote sensing the products are limited to the 2 dimensional planar abstraction of surface topography. Despite their geometrical deformations spectral Remote Sensing methods offer more effective and economical ways for such mapping practices.

3.1 Remote Sensing Technologies and ASTER Sensor

With the fast progress in the field of RS and advances in satellite technology since the launch of Landsat in 1972, it became a very useful way to employ RS technologies. The advantages of satellite imaging systems are recognized and applications are widespread such as; mapping rock units (stratigraphy), monitoring the expression and modes of the origins of landforms (geomorphology), determining the structural measures such as folds and faults (structural geology), evaluating natural events, e.g., landslides, floods, volcanic eruptions (hazards) and seeking alteration and other indications of mineralization, to subsurface deposits of ore minerals, hydrocarbon exploration and groundwater.

Moreover, RS technologies provide cost-effective and multipurpose image data. Information about surface characteristics can be obtained globally and maintains as an advantage especially when work is carried out in areas that are difficult to access. There is an extensive variety of data available in the market including numerous sensors with varying spatial, spectral, and radiometric resolutions.

An advantage of ASTER data is the unique combination of wide spectral coverage and high spatial resolution in the VNIR through SWIR to the TIR regions (Gad and Kusky, 2007). ASTER data are collected in 14 bands, three in the visible and near-infrared (VNIR) portion of the electromagnetic spectrum with 15 m spatial resolution, six in the short-wave infrared (SWIR) with 30 m spatial resolution, and five in the thermal infrared (TIR) with 90 m spatial resolution. Therefore, these data enhance the capability of lithological discrimination between the different rock units. Because of this advantage, ASTER simulation and data have been used increasingly for geological mapping (e.g., Rowan and Mars, 2003, Qui et al., 2006). The radiometric characteristics of the sensor are given in Table 3.1:

Table 3. 1: ASTER instrument characteristics

Region of spectrum	Band No.	Spectral Range (μm)	Spatial Resolution
VNIR	1 2 3N 3B	0.52 - 0.60 0.63 - 0.69 0.78 - 0.86 0.78 - 0.86	15m
SWIR	4 5 6 7 8 9	1.600 - 1.700 2.145 - 2.185 2.185 - 2.225 2.235 - 2.285 2.295 - 2.365 2.360 - 2.430	30m
TIR	10 11 12 13 14	8.125 - 8.475 8.475 - 8.825 8.925 - 9.275 10.25 - 10.95 10.95 - 11.65	90m

ASTER measures reflected radiation in three bands between 0.52 and 0.86 μm (VNIR) and in six bands from 1.6 to 2.43 μm (SWIR), (Fujisada, 1995). ASTER also has a back-looking VNIR telescope. Thus, stereoscopic VNIR images can be acquired at 15m resolution. In addition, emitted radiation is measured in five bands in the 8.125 to 11.65 μm wavelength region (TIR) (Rowan et.al., 2005).

However there are unexpected features which can effect the quality of the image. One of these is the Crosstalk effect, which qualitatively worsens the image. Largest effect is in band 4 into 5 and 9. It is an effect in ASTER imagery caused by signal leakage from band 4 into adjacent bands 5 and 9. Incident light to band 4 detectors is reflected at aluminum coated parts and reaches to the detectors of other bands by multi-reflection in the cavity between detector plane and bandpass filter. In other words, not all light hitting the detector is absorbed and it is reflected. Some of the reflected light is reflected back down by the filters. If the amount of light leaking from one pixel to each other pixel in all the SWIR bands is known, it can be corrected (http://asterweb.jpl.nasa.gov/content/05_bibliography/03_ Workshop/ presentations/rad-cal-biggar.ppt#31).

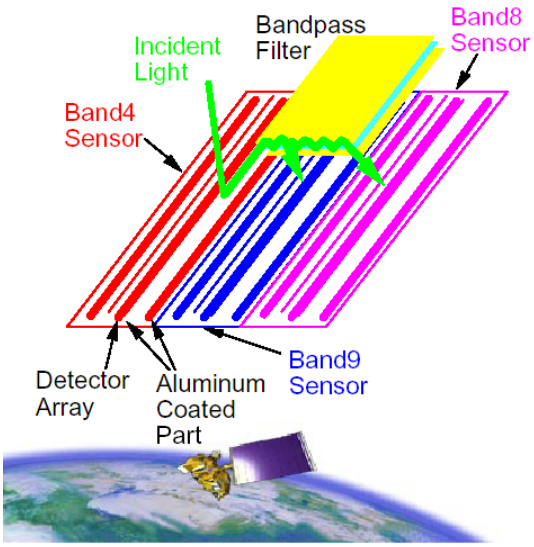

Figure 3. 1: Representation of crosstalk effect (http://asterweb.jpl.nasa.gov/ content/05_bibliography/03_Workshop/ presentations/rad-cal-biggar.ppt#31)

Here, it is important to mention that although the image used in this study was obtained before 2007, related with the SWIR data, it is reported that some anomalous saturation of values has been observed in ASTER Bands 5 through 9 since May 2007. In the ASTER Terra website (http://asterweb.jpl.nasa.gov/swir-alert.asp), users are advised that for ASTER SWIR data collected between late May 2007 and late January 2008, the SWIR detector temperature exceeded the normal 83ºK and SWIR data acquired during these periods may exhibit anomalous saturation of values, particularly at high sun angles and for materials that are highly reflective in the SWIR bands. VNIR and TIR bands are unaffected by this problem.

3.2 Geological mapping using ASTER

Analysis of basic elements of an image; *texture, tone, pattern, shape, size, shadow* and *association*, can reveal the geology of an area (Outtara et al.,2004). Geological information which can be extracted from an image is mainly rock types and structures of an area and the above terms influence these. In the following sections, literature is reviewed and the methodologies utilized for mapping are explained.

3.2.1 Band Combinations

Examining the data with different band combinations includes RGB and IHS images. For the study area, as it is explained in Chapter 4, the most useful band combination in delineating geological units was 4-3-2 combination in RGB packing order (Figure 3.2).

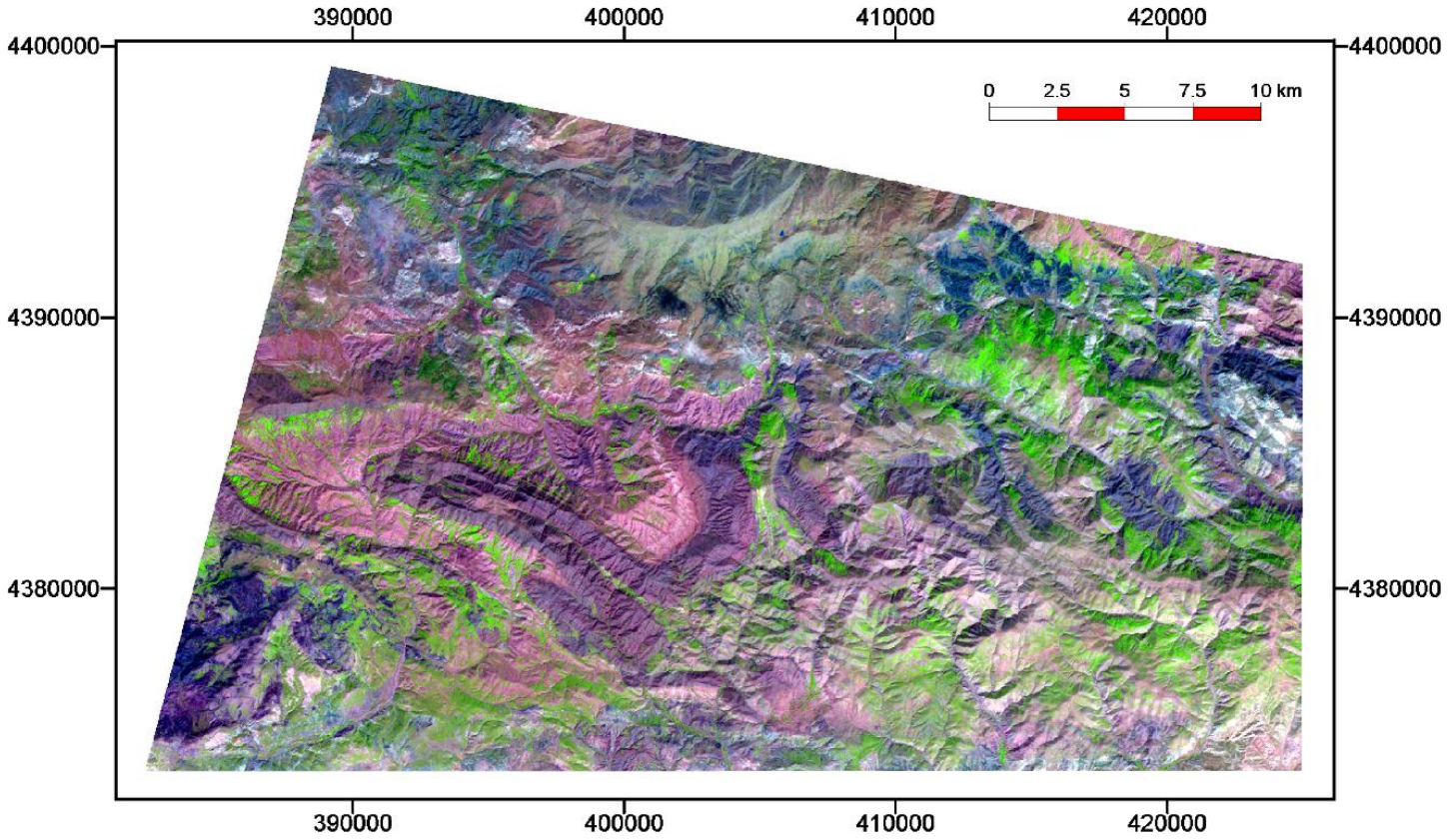

Figure 3. 2: Band combination of 4-3-2 for the study area

3.2.2 Principal Components Analysis

A common method adapted from multivariate statistics, for use in remote sensing analysis, is principal components analysis (PCA), which describes an image by new orthogonal axes, or principal components (Lillesand and Kiefer, 2004).

Gomez et al., 2005 utilized VNIR and SWIR data (9 ASTER bands) for geological application. A Principal Component Analysis (PCA) has been realised and it is stated that PCA results enable the validation and the revision of the lithological boundaries defined on previous geological maps and provide information for characterising new lithological units corresponding to surficial formations previously unrecognised. In addition, supervised classification is calculated from both PCA results and based on the geological map which showed that processing of ASTER remote sensing data set can be used as a powerful tool for geological mapping.

3.2.3 Band Ratios

Ratio images have been used extensively as a computationally rapid means of displaying compositional information while subduing reflectance related to albedo and topographic slope variations (Rowan et al., 1974; among others).

ASTER band-ratio combinations and band math are effective in emphasizing spectral characteristics of certain rocks and minerals and hence are more effective in lithological mapping compared to the RGB band combination images (Rowan and Mars, 2003; Rowan et al., 2005). Band ratio, in other words an ”index” is utilized for extraction of gypsum units in the region. The procedure is explained in Chapter 4.

3.2.4 Multi-Spectral Image Classification

Image classification is a method that converts the image data to thematic data by grouping features. This grouping is basically done by assembling the features similar to each other and separating the dissimilar ones. Class labels are assigned to each pixel thus resulting in a manageable size of classes. In multi-spectral image classification the spectral information represented by the digital numbers in one or more spectral bands are used and each individual pixel is attempted to be classified based on this spectral information.

Two approaches are possible in definition of the groups or clusters: supervised classification and unsupervised classification. In a supervised multispectral classification, the operator specifies the classes that will be used. In an unsupervised multispectral classification, the computer specifies the classes that will be used (Sabins, 1999). In spite of training data selection being a routine process, supervised approach is generally preferred since it gives more accurate class definitions and high accuracy in comparison with unsupervised approach (Tso and Mather, 2001).

Several classification algorithms are present. The choice of algorithm depends on the purpose of the classification and the characteristics of image and training data. In practice Minimum Distance to Mean and Maximum Likelihood classifiers are used widely (Kerle et al.2004).

Maximum Likelihood Classification

The method assumes a Gaussian relationship between input variables and class probabilities, and calculates class probabilities as functions of mean vectors for each class (i.e. for each class the mean value of training samples in each input variable is calculated) and the co-variance matrix for the input variables in each class.

Therefore, 'training' the algorithm simply involves calculating the mean vector and co-variance matrix for each class (Kerle et al.2004).

3.3 Terrain Analysis Methods and Terrain Parameters

Topography provides insight into the local tectonic and sedimentary history. One of the best ways to analyze and quantize topography is to work with DEMs, which allow a quick analysis of the area-altitude distribution of land.

Jordan et al. (2005) provides an overview of methods for the extraction of morphotectonic features from DEMs and to develop a systematic procedure for the application of these methods to morphotectonic terrain analysis.

Brown et al. (1998) showed the ability of geomorphic measures i.e. elevation, relative relief, roughness, and slope gradient, derived DEMs to differentiate glaciated landscapes using maximum likelihood classification and artificial neural networks (ANN). Different classification trials were conducted to assess the contribution of using morphometric variables in classification. The work showed that the form of land surface could be used to identify types of landscapes that are genetically different.

Frohn (2006) suggested that the application of landscape metrics can be a useful tool in remote sensing image classification when the features of interest have similar spectral properties but differing shape or spatial properties. He used landscape shape complexity metric, in image classification. In addition he mentioned other metrics which capture spatial patterns of patches on the landscape such as measures of fragmentation, clumping, asymmetry, density, core-area, and compactness.

Grohmann et al. (2007) proposes an evaluation of SRTM data applicability in geomorphology and morphotectonic analysis, considering the morphometric parameters slope, aspect, surface roughness and isobase surface. The morphometric indices evaluated showed the correlation of landscape within an alkaline massif with structures with different trends, as well as landforms related with recent tectonic influence.

CHAPTER 4

DATA PROCESSING AND ANALYSIS

The objective of this chapter is to study whether different geological units in the region can be separated from each other only by using ASTER image data and if integration of ancillary data results in improvement of the results.

Image processing methods are applied to ASTER data for extraction of relevant information and mapping geologic features. The overall methodology is represented in Figure 4.1

4.1 Pre-Processing of Images

SWIR bands of the image were resampled to VNIR pixel size, which is 15m; so that these bands can be combined with VNIR bands and geologic structures can be interpreted from different channels.

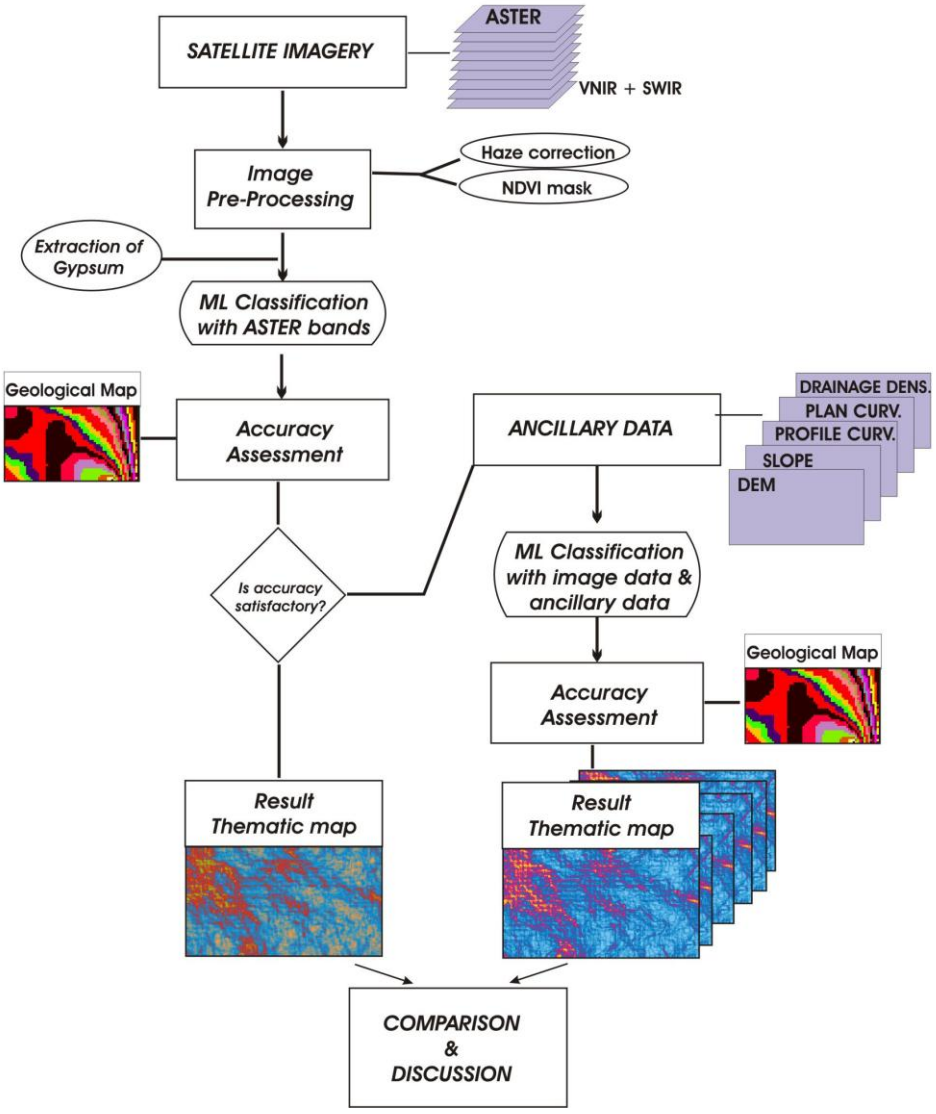

Figure 4. 1: Flowchart of the study

Haze correction was done by dark pixel subtraction method for the VNIR bands. The minimum value in each band is taken to represent or approximate the effect of atmosphere and removed from each band (Table 4.1).

Table 4. 1: Removed values for haze correction

ASTER band	Removed value
1	37
2	24
3	20

Since vegetation have an effect on the observation of spectral properties-reflectance of underlying rocks, vegetation effect is masked from each band using NDVI (normalized difference vegetation index) before any image processing is done for geological mapping. False color image displays the areas covered with vegetation in tones of red (Figure 4. 2). By examining the false color image vegetated areas to be masked are chosen, a threshold value is determined from the NDVI image to pick out these areas and was used in preparing the mask (Figure 4.3).

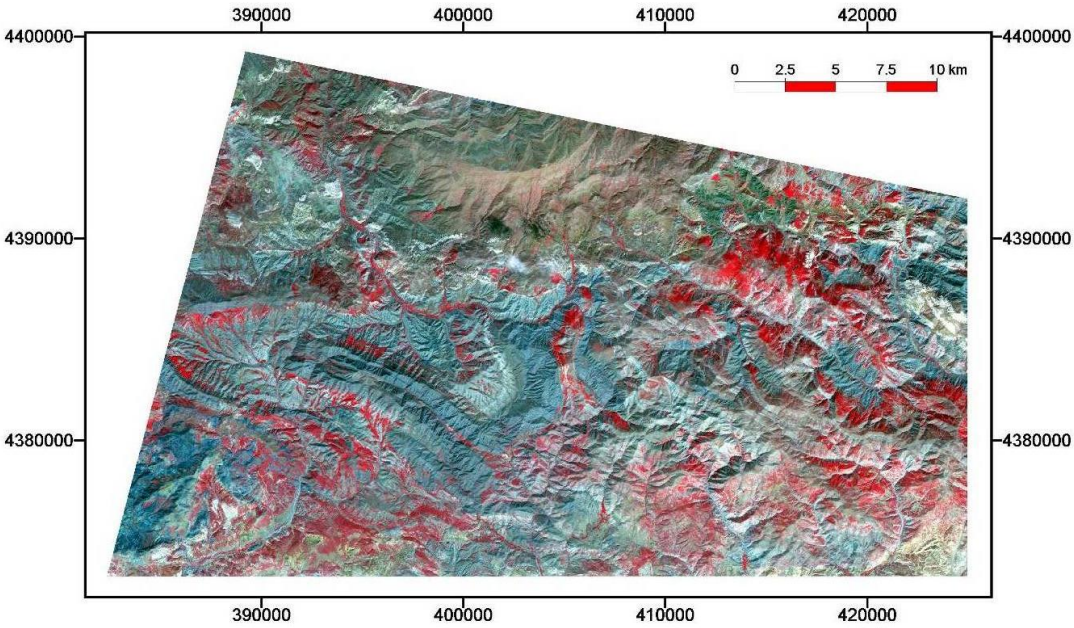

Figure 4. 2: Band combination of 3-2-1 in RGB for the area, red areas show vegetation.

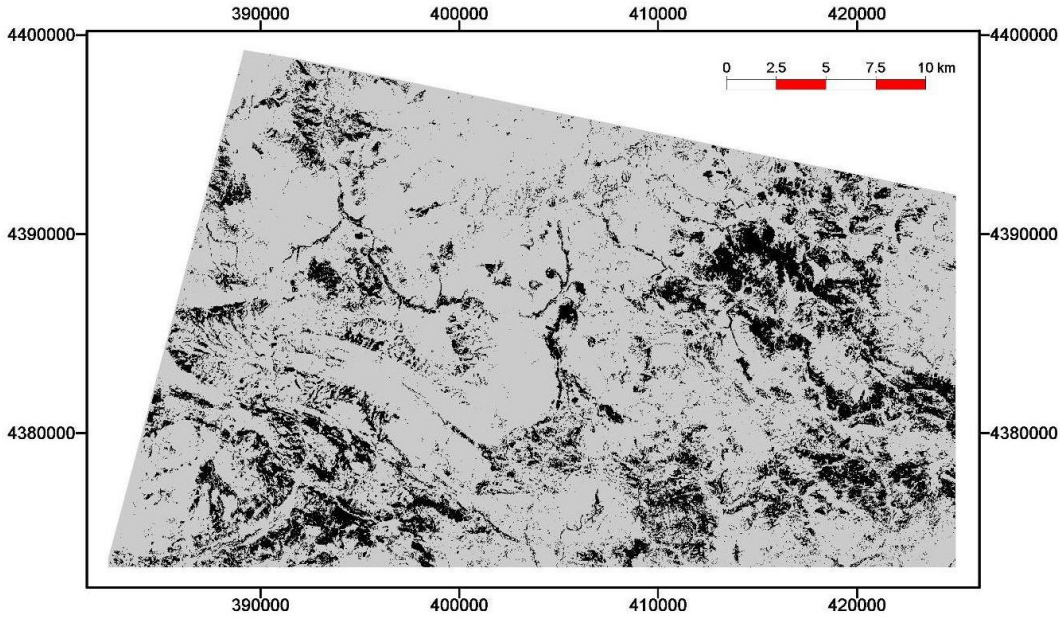

Figure 4. 3: Vegetation mask prepared using NDVI, black areas are masked

4.2 Analysis

Following the pre-processing step, (haze correction and masking of vegetated areas) image classification is performed.

Since vegetation cover is not very dense in the study area except evident forest clusters and sparse vegetation existing in the SW parts of the area (masked during image pre-processing stage) lithological units can be identified and mapped as much as the spectral and spatial resolution of the sensor and existing dataset enables. In addition, when selecting the classes that will be used in the classification an assumption is made taking into consideration, the definition of "Formation". Namely, "Formation" is defined as having a homogeneous lithology or having extreme lithic heterogeneity where such heterogeneity constitutes a form of unity that differentiates from adjacent rock units. Therefore each formation polygon extracted from the 1/100000 scale geological map is a separate class in the classification.

In the analyses of remote sensing datasets, the 1/ 100000 scale geological maps (georeferenced and digitized) are used as reference data. This geological map is the only geological reference data which is used as base for this research in addition to the literature data. The generalized geological map is given in Figure 4.5. Geological units obtained from the above mentioned map, which are used as the classes in the training set are given in Table 4.2.

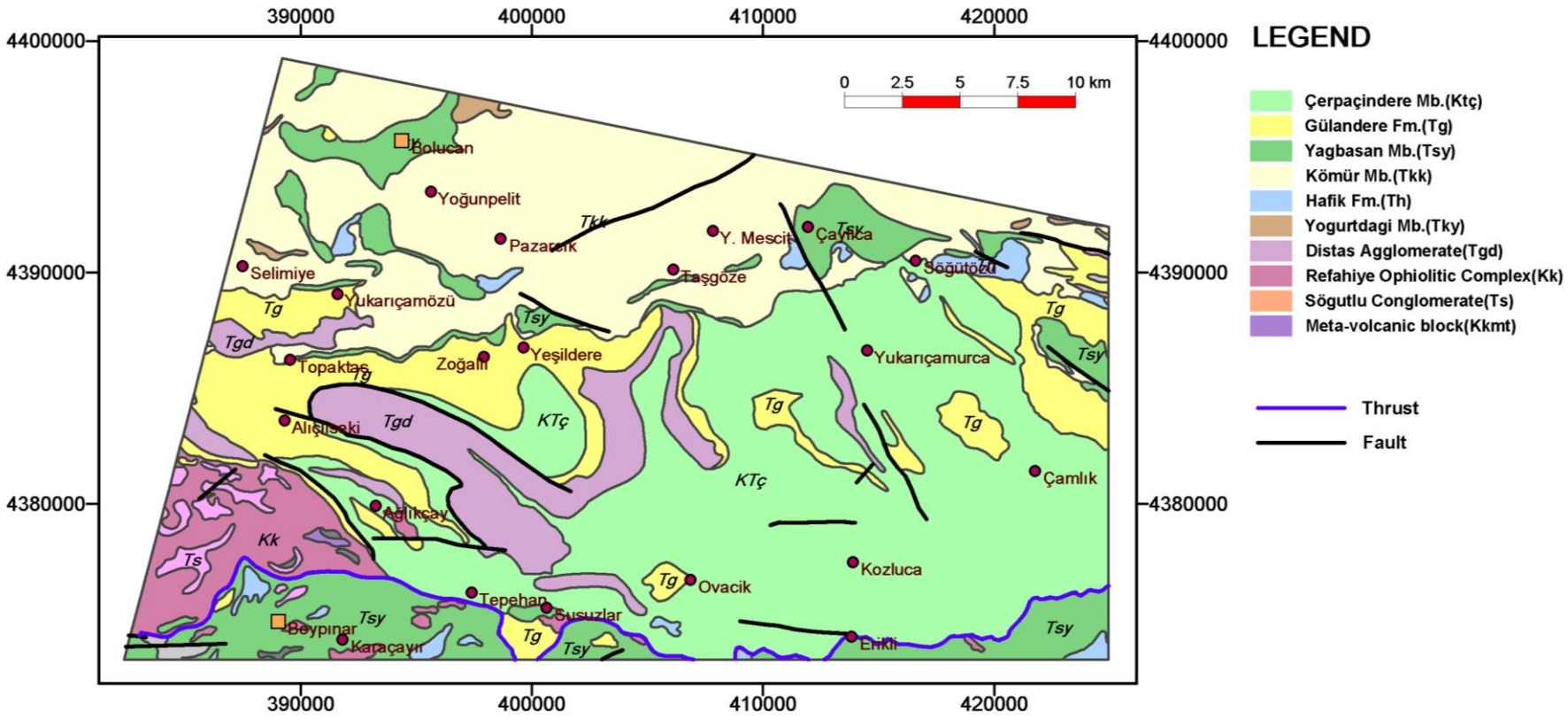

Figure 4. 4: Generalized geological map

Table 4. 2: Table showing the geological units present in the area

Code	Symbol	Explanation	Formation	Lithology
1	KTt	Tecer limestone	Tecer limestone	limestone
2	Ktç	Çerpacin member	Cerpacindere Fm	sandstone, conglomerate, claystone, clayey limestone, sandy limestone and tuff
3	Kk	Refahiye ophiolitic complex	Refahiye oph.complex	dunite, peridotite, serpentinite, amphibolite, gabbro and serpentinization
4	Kkm	Crystalized limestone block	Refahiye oph.complex	crystallized limestone
5	Kkmt	Meta-volcanic block	Refahiye oph.complex	meta-volcanite outcropping with Jurassic limestones
6	Kkr	Radiolarite block	Refahiye oph.complex	radiolarite-serpantinite-calicite veins-spilite
7	Tg	Gulandere Fm	Gulandere Fm	turbiditic flysh character consists of successions of sandstone, claystone, conglomerate, siltstone, tuffs and agglomerates (Dištaş agglomerate).
8	TgKk	Ophiolite block	Gulandere Fm	Refahiye ophiolitic complex.
9	Tgd	Distas aglomerate	Gulandere Fm	aglomera
10	Tgm	Crystalized limestone block	Gulandere Fm	marble

Table 4.2 (cont'd): Table showing the geological units present in the area

11	Th	Hafik Fm	Hafik Fm	dominant rock unit of gypsum is formed by white coloured gypsum and successions of multicoloured (red, dark red, green, blue) claystone and sandstone.
12	Tkk	Komur member	Kemah Fm	successions of sandstone, claystone, mudstone, clayey limestone and siltstone
13	Tky	Yogurtdagi member	Kemah Fm	limestones, calcite veined
14	Tkç	Çakiltasi member	Kemah Fm	reddish, green, in places grayish coloured, clay and carbonate cemented, good sorted conglomerate and sandstones
15	Ts	Sogutlu conglomerate	Sogutlu conglomerate	serpentinite conglomerate Serpentinite cement is replaced by carbonate sediments in upper levels
16	Tsy	Yagbasan member	Selimiye Fm	successions of sandstone, claystone, mudstone, gypsum and conglomerate
17	TsyKk	Ophiolite block	Selimiye Fm	ophiolite
18	Tsyg	Gulandere Fm block	Selimiye Fm	Gulandere Fm block
19	Tsym	Crystalized limestone block	Selimiye Fm	marble
20	Tsyr	Radiolarite block	Selimiye Fm	radiolarite

4.2.1 Spectral Bands (ASTER) classification

The Maximum Likelihood Classification (MLC) was chosen among other classification methods to be utilized in the classification. This is due to the fact that in MLC, every pixel in the image is assigned to the class of highest probability. Therefore it can be said that MLC considers variability within cluster-class variability**,** the shape, the size and the orientation of clusters. The mean vector and covariance matrix are used to calculate a statistical distance, which is used to characterize each class. Selection of sample size that is sufficient to provide for an unbiased and efficient estimate of these parameters is important. (Tso and Mather, 2001)

A descriptive analysis of the statistics of the DN values for each unit, according to the published 1/100000 scale geological map, is undertaken. Analysis is carried out to determine which of the individual spectral bands of ASTER data are useful in multi-spectral classification of lithologic units from remotely sensed dataset.

Figure 4.5 shows the normalized mean DN values for different units in single bands of ASTER. From the figure it can be said that Tg and Ktç, Tkk and Tsy show similar characteristics in most of the bands and are not discernable from each other in ASTER multispectral data. Likewise, Ts and Kk also show similar trends. Although these units show similar reflections and are likely to be mixed in the classification, ASTER SWIR bands are effective in lithological mapping since many sedimentary rocks have distinctive spectral features in this portion of the electromagnetic spectrum (Evans, 1988).

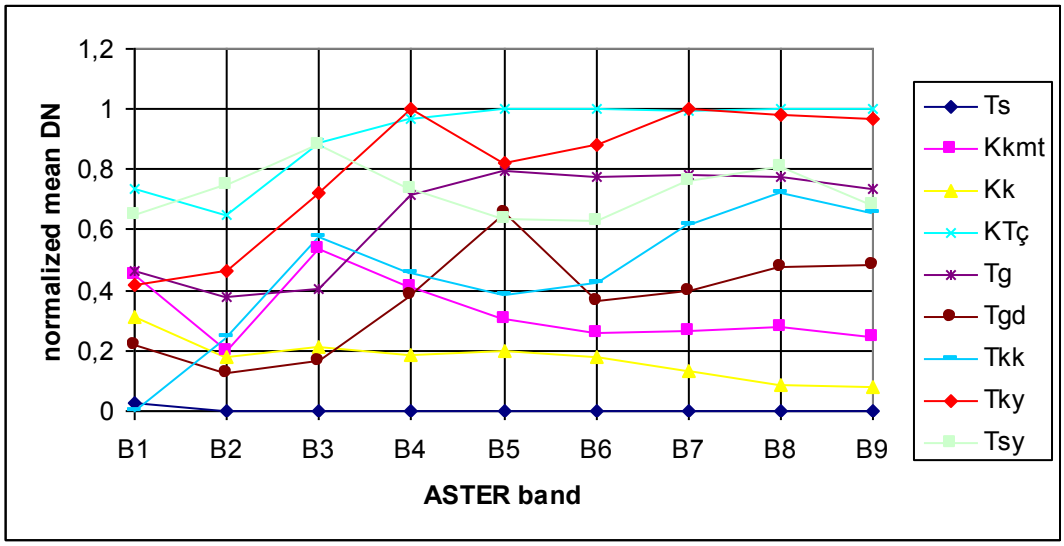

Figure 4. 5: Normalized mean DN values of units in ASTER bands

For example within SWIR region, limestones and shales are spectrally distinctively different. The limestones have a dominant absorption feature close to 2.3 mm which corresponds to band 7 and 8 of the ASTER data (Figure 4.6). On the other hand, shales have flat reflectance spectra within these wavelengths (Figure 4.6).

Moreover, shales are characterized by low total reflectance compared to limestones. ASTER Band 7 data is effective in distinguishing clay minerals since these have a significant absorption feature within these bands (Sabins, 1997). Band 3 of ASTER data is effective in mapping iron oxides since these minerals have high reflectance in this band.

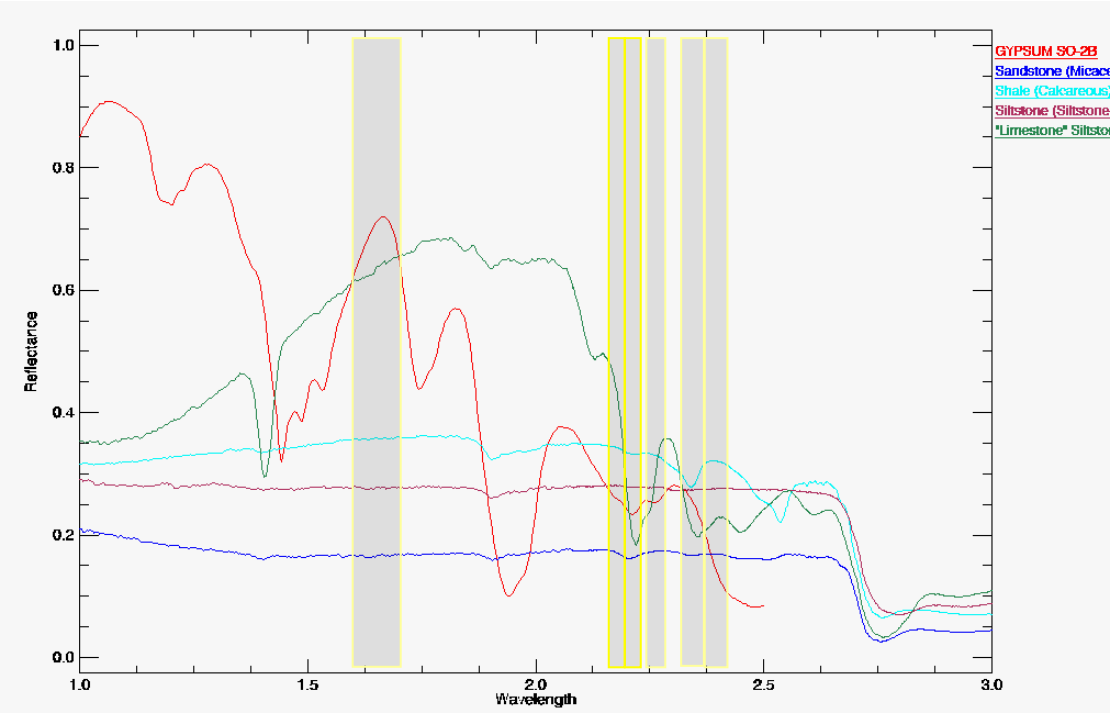

Figure 4.6: Spectral reflectance curves of dominant lithologies in the study area for SWIR bands. The spectral curves are extracted from the Jet Propulsion Laboratory (JPL) Spectral Library. Location of ASTER bands are shown with gray bars on the top of figure. (Baldridge et al.,2009)

4.2.1.1 Extraction of Gypsum

In the study area two of the mapped units contained rock unit of gypsum. Hafik formation is dominated by gypsum and Yağbasan member contains successions of gypsum in addition to clastics.

As an approach to classify these units, picking these out by spectral indices are more practical. Sulfate index modified from Quartz index (Ninomiya, 2002) for TIR region is shown to be successful for gypsum minerals (Öztan, 2007).

Sulfate Index is given as:

$$\text{Sulfate Index} = \frac{B\ 10 * B\ 12}{B\ 11 * B\ 11} \qquad \text{(Öztan, 2007)}$$

ASTER image TIR bands resampled to 15 m pixel size and georeferenced to the same datum with the other bands were used to calculate the index image. In the resultant sulfate index image, positive anomalies for sulfate minerals are reflected as bright pixels (Figure 4.7). These pixels were selected by defining a threshold and a gypsum mask was prepared (Figure 4.8) in order to mask these areas before classification.

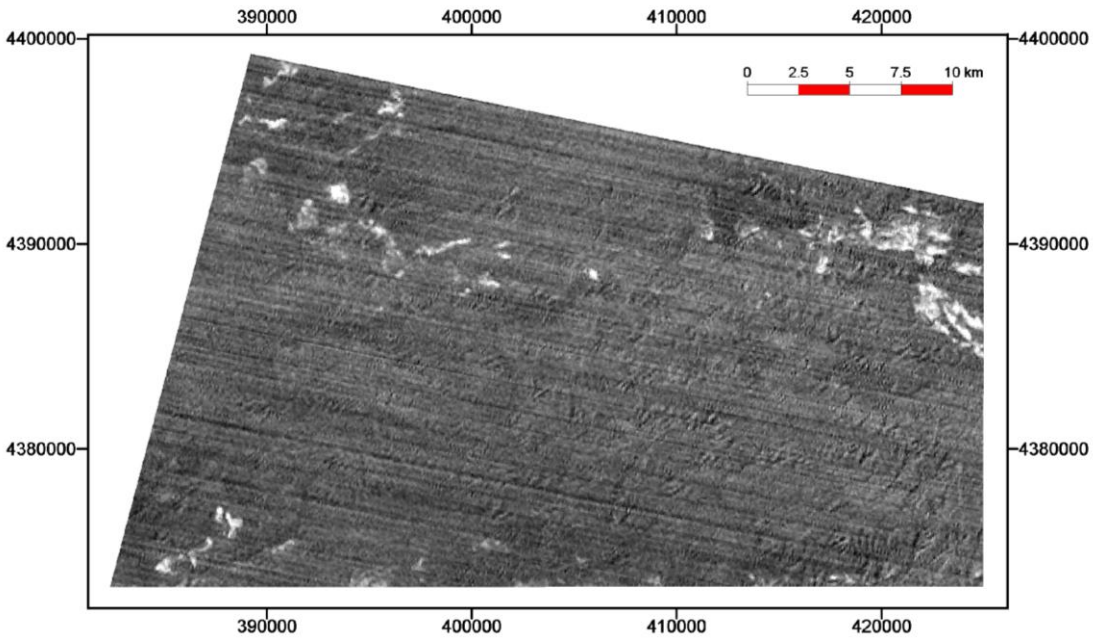

Figure 4.7: Resultant Sulfate Index image, bright pixels show gypsum

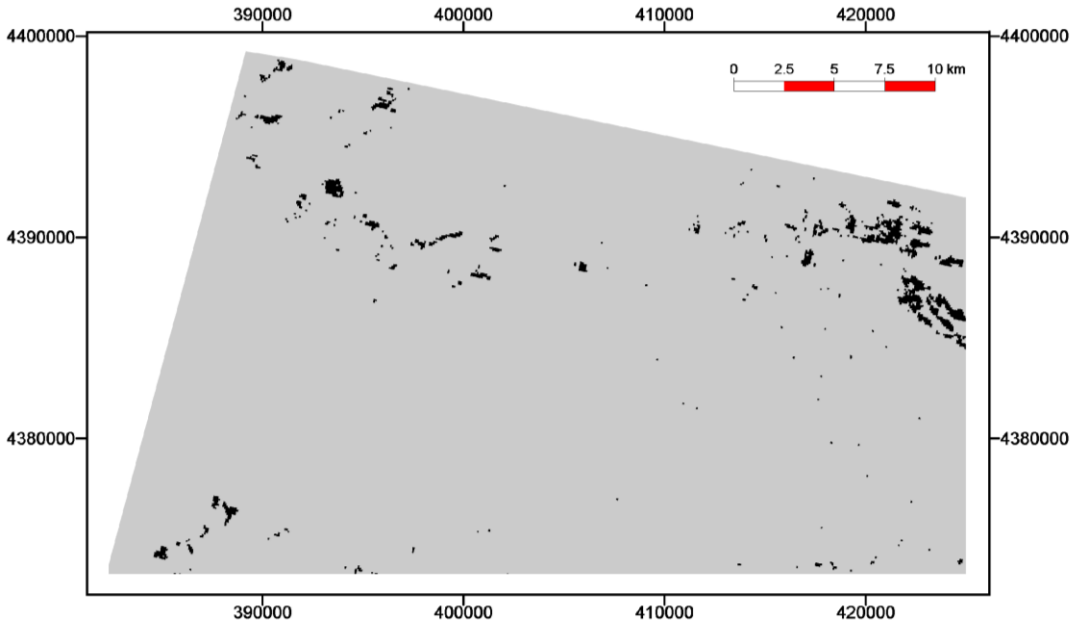

Figure 4. 8: Mask prepared for gypsun units, black areas are masked

4.2.1.2 Training and Validation set selection

Supervised classification collects groups that have similar spectral signatures to be applied to the entire scene. In addition, supervised classification requires that the operator to be familiar with the area of interest. Therefore it is assumed that all lithologies to be mapped within the classified scene are already known.

Geological map is used as a guide in the training process and validation of the analysis of remote sensing dataset. Red, green, blue (RGB) colour combinations of bands are used to display the spectral characteristics of lithological units. Before image classification is performed, different band combinations were employed to make an initial visual interpretation to guide to discriminate different lithological classes. The most helpful combination is found to be the 4-3-2 combination in RGB packing order.

Sample pixels are selected from the image in order to represent each class properly. An error set was used to validate classification. Since there is no ground truth data available at the time of study, random sampling was used for generation of miscellaneous control points. Firstly, training areas were selected proportionally with the area of the class polygons. Then from these selected points, two third of them were randomly picked out to form the training set, whereas the rest one third was used for error set (Table 4.3). In doing so, the reference geology polygons were used and for each class test sites were determined by randomly placing points in each polygon. In addition, review of geological map and the classification result were interpreted qualitatively and the conditions of classes are analyzed.

Table 4.3: Number of pixels of training and error sets

Class	Training set	Error set
Refahiye Oph. Complex (Kk)	77	28
Meta-volcanic block (Kkmt)	17	11
Çerpaçin Mb. (KTç)	110	80
Yağbasan Mb. (Tsy)	71	52
Kömür Mb. (Tkk)	125	70
Gülandere F. (Tg)	117	51
Dişţaş agglomerate (Tgd)	107	37
Söğütlü conglomerate (Ts)	42	14
Yoğurtdağı Mb. (Tky)	60	20

4.2.1.3 Classification of the area

Once the training process was completed, the MLC was applied to the original 9 ASTER spectral channels that were already processed previously for atmospheric effects and vegetation. The classification scheme used for image interpretation consisted of 9 classes. Analysis was limited to geological units covering a total area of at least 1 km^2 in order to ensure a reasonable sampling density and the units which are designated as blocks are not attained as separate classes. The weights of all the classes were assumed equal and apriori probabilities were not considered. The definition of each class and the classification result is given in Table 4.4 and Figure 4.9 respectively.

Table 4. 4: Classes used in classification

No.	Label
1	Refahiye ophiolitic complex (Kk)
2	Meta volcanic block (KKmt)
3	Çerpaçin Mb.(KTç)
4	Yağbasan Mb. (Tsy)
5	Kömür Mb.(Tkk)
6	Gülandere Fm. (Tg)
7	Distaş agglomerate (Tgd)
8	Söğütlü conglomerate (Ts)
9	Yoğurtdağı Mb. (Tky)

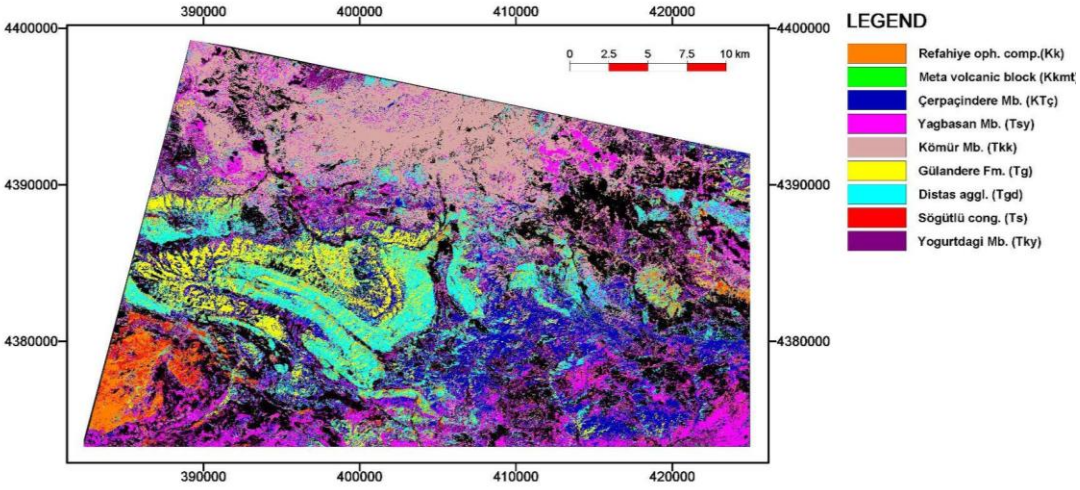

Figure 4. 9: Result of classification with nine ASTER bands

Accuracy of the classification gives the ratio of correctly assigned pixels to the misclassified pixels. The classification accuracy is depicted in the error matrix between training and error sets. The error matrix of classification with nine ASTER bands is given in Table 4.5.

Table 4. 5: Error matrix of classification with nine ASTER bands

ES / TS	Kk	Kkmt	Ktç	Tsy	Tkk	Tg	Tgd	Ts	Tky	Total	Acc. (%)
Kk	7	5	2	2	0	0	0	7	0	21	33,33
Kkmt	0	3	0	0	0	0	0	0	0	3	100
Ktç	2	0	53	7	0	6	0	0	1	69	76,81
Tsy	0	0	3	32	10	0	0	1	3	49	65,31
Tkk	0	0	18	16	57	4	0	0	2	97	58,76
Tg	1	0	5	0	0	33	12	0	0	51	64,71
Tgd	2	1	1	0	3	7	22	0	0	36	61,11
Ts	11	0	0	0	0	0	0	4	0	15	73,33
Tky	5	2	0	5	4	1	0	0	14	31	45,16
Total	28	11	80	62	74	51	34	12	20	372	
Acc.(%)	64,29	27,27	66,25	51,61	77,03	64,71	64,71	0	70		
Overall Acc.(%)	62,37										

For the classification with nine ASTER bands, overall accuracy is 62, 37% where Kömür member and Yoğurtdağı member shows relatively good correlation with reference to the published geological map. The Söğütlü conglomerate unit and meta-volcanic block showed very low accuracies. This can be due to the small areal coverage of these units.

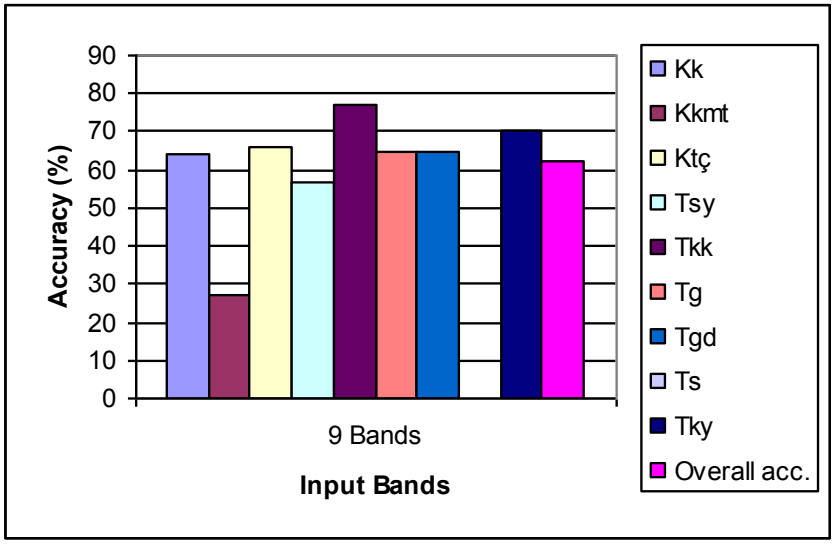

Figure 4. 10: Classification accuracy for each class (Kk: Kömür Mb., Kkmt: Meta-volcanic block, Ktç: Çerpaçindere , Tsy: Yağbasan Mb., Tkk: Refahiye Oph. Complex, Tg: Gülandere Fm., Tgd: Dištaş Agglomerate, Ts: Söğütlü Conglomerate, Tky: Yoğurtdağı Mb.)

4.2.2 Ancillary Data Integration

Analyzing diverse data sets together, it is possible to extract better and more accurate information in a synergistic manner than by using a single data source alone (Outtara et al. 2004).

For incorporating ancillary data in the classification process Hutchinson (1982) has suggested three methods: pre and post- classification techniques and classifier operations. Typically ancillary data are derived from digital topographical maps, elevation models and thematic maps (Kam, 1995).

In view of the fact that shapes of various types of lithologies may differ when mechanisms of deposition vary, it is hypothesized that different types of lithologies would be differentiable, to some extent, by surface morphology. Moreover, topographic data can be integrated with other spectral data for perspective visualization of unknown terrain, introduction of relief displacement into remotely sensed image in order to provide stereo-optic viewing potential and the correction of remotely sensed data for variable solar illumination (Drury, 2001). An objective was to identify the degree to which this was true. Five variables were calculated from the DEM in order to describe the surface morphology in the study area. The DEM used was generated by interpolating values of contour lines using minimum curvature surface fitting algorithm with the default parameters. The Minimum Curvature method applies a two dimensional cubic spline function to fit a smooth surface to the set of input elevation values. The computation requires a number of iterations to adjust the surface so that the final result has a minimum amount of curvature (TNT User Manual).

Although there are many parameters that can be derived from DEM or that can be used as ancillary data, a limited number of parameters which are assumed to reflect the underlying lithologies must be selected. This selection is mainly based on experience of previous mapping experiences and on geomorphological considerations. List of morphometric terrain parameters that were selected are given in the table below:

Table 4. 6: Morphometric terrain parameters and explanations

Parameter	Explanation
Slope	Rate of change of elevation
Profile curvature	Curvature in the vertical plane parallel to slope direction
Plan curvature	Curvature of a contour line formed by intersecting a horizontal plane with the surface (contour curvature)
Drainage density	density of drainage network

-***Elevation*** is assumed to be an identifier of the lithologies since differential erosion of rocks results in differences in elevation of landforms.

-***Slope*** is considered as an important input since it shows steepness of the surface and it is useful to consider slope as a measure of change in a surface. These changes might reflect the change in underlying geology.

-***Slope concavity/ convexity*** maps can be derived as the second derivative of a DEM, or in other words, as the change of slope (Wilson and Galant, 2000 and TNT User Manual).

-***Plan curvature*** is the curvature of slope that is parallel to the elevation contours which can be used to identify divergent or convergent flow areas on the landscape; convergent flow generally indicates higher erosion and transport potential while for divergent vice versa.

-Profile curvature is the curvature of the surface perpendicular to the elevation contours. This parameter indicates the rate of change of slope and therefore influences the flow velocity of water draining the surface and thus erosion and the resulting downslope movement of sediment.

-Drainage density is defined as river length per unit area and is primarily related to resistance of rock to erosion, while resistance to erosion is related to permeability.

-Although ***aspect*** was also considered for addition in the analysis, it is anticipated that among other variables its effect would not be revealed.

Nevertheless, it is important to mention that classification and description of geomorphic features is a different field by itself and therefore not emphasized in this study.

From the ASTER data displayed in different combinations it can be seen that there are significant differences in surface mineralogy and roughness of regions underlain by different lithologic units. This infers that for different lithologic units, due to the different compositions resistance to weathering and surface runoff will be different and therefore, result in different topographic features.

Image classification was performed based on synthehic ancillary data layers mentioned in the above paragraphs together with the nine ASTER bands. In practice any classifier can be employed and in addition to the spectral bands and terrain parameter maps can be used as input. All the ancillary data layers were resampled to ASTER band pixel size and band extents in order to be put in the classification.

4.2.3 Classification with Terrain Parameters

The training set was re-classified by adding DEM, slope, plan and profile curvature drainage density stepwise and all five rasters together to the 9 ASTER bands. For each class, classification accuracy was evaluated and plotted for the different image variables.

4.2.3.1 DEM

DEM generated from digitization of 1/25000 scale topographic maps was used as the source for elevation values and terrain data derived in the study. DEM was generated by interpolating values of contour lines using minimum curvature surface fitting algorithm with the default parameters. During the DEM production process, the output was selected to be 8bit and an ASTER band was selected as a reference image so that this layer is compatible to be used as input together with the ASTER spectral bands. Elevation of the study area obtained from the DEM (Figure 4.11) ranges from 1244 to 2800 m. The value ranges for each formation is given in Figure 4.12 and the maximum elevation is observed in the Kömür (Tkk) member.

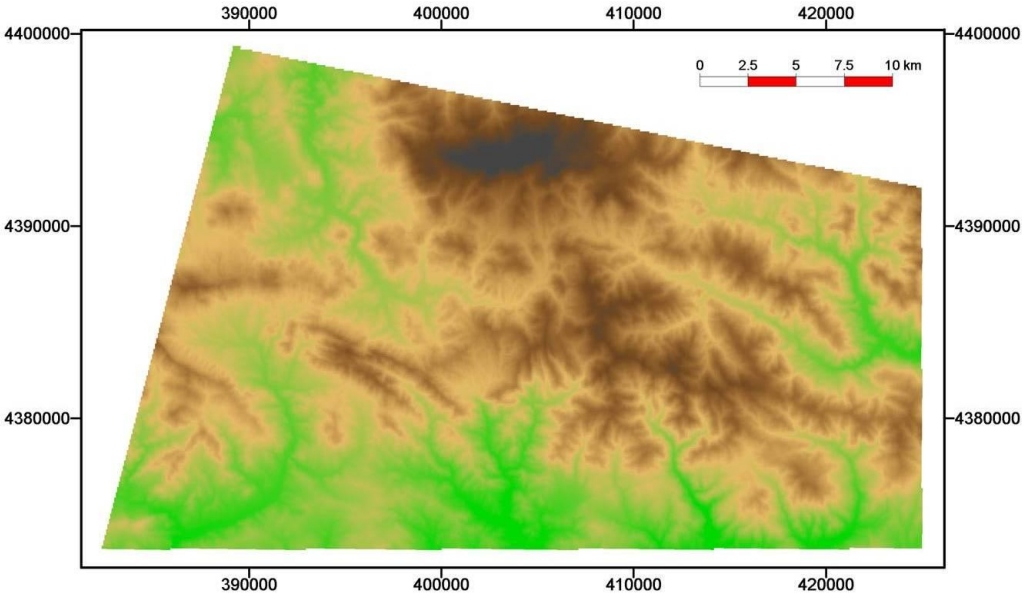

Figure 4.11: Digital Elevation Model of the study area

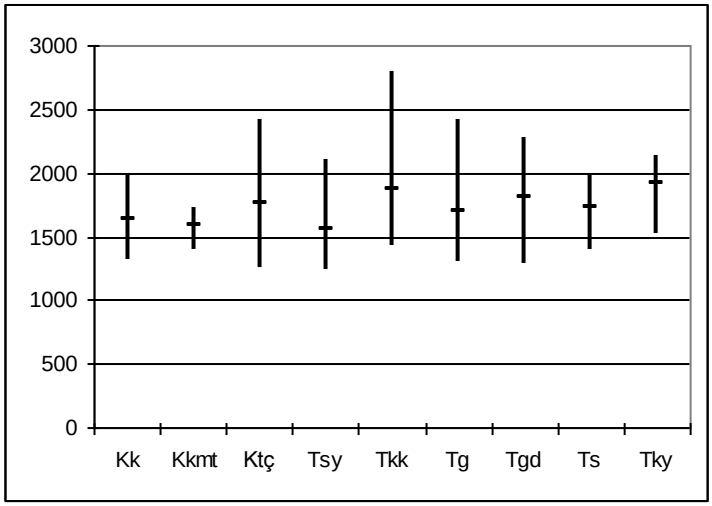

Figure 4. 12: Elevation value ranges for each formation.

The classified image is given in Figure 4.13 and error matrix for this classification in Table 4.7 .Visual interpretation shows limited distribution of Gülandere formation and more areal distribution of Çerpaçin member in comparison to the nine band classification. The classification accuracy for Gülandere formation is lower than in the nine band classification since the elevation in this unit does not a show strong discriminating character.

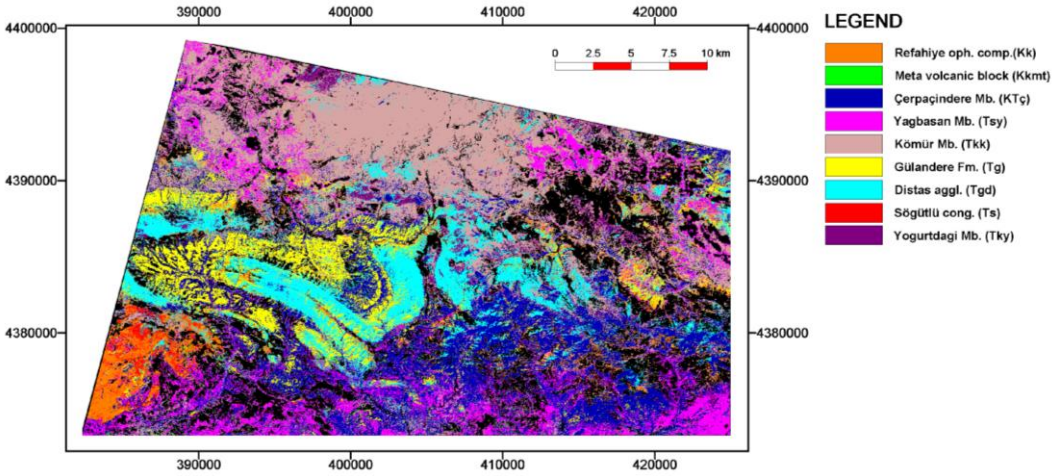

Figure 4. 13: Result of classification with 9 ASTER bands with DEM

Table 4. 7: Error matrix of classification with nine ASTER bands and DEM

ES / TS	Kk	Kkmt	Ktç	Tsy	Tkk	Tg	Tgd	Ts	Tky	Total	Acc. (%)
Kk	8	2	0	0	0	0	0	7	0	17	47,06
Kkmt	0	5	0	0	0	0	0	0	0	5	100
Ktç	2	0	54	6	0	6	0	0	4	72	75,00
Tsy	0	3	0	35	6	1	0	0	0	45	77,78
Tkk	5	0	21	17	59	5	0	0	2	109	54,13
Tg	1	0	1	0	2	31	7	0	0	42	73,81
Tgd	0	1	1	4	2	8	27	0	0	43	62,79
Ts	12	0	1	0	0	0	0	5	0	18	66,67
Tky	0	0	2	0	5	0	0	0	14	21	66,67
Total	28	11	80	62	74	51	34	12	20	372	
Acc(%)	71,43	45,45	67,50	56,45	79,73	60,78	79,41	0	70		
Overall Acc(%)	65,86										

However, the accuracy of Dištaş agglomerate is increased from 64,71% to 79,41%. Also there is 6% increase in accuracy for the Refahiye Ophiolitic complex unit and these can be attributed to the high internal relief of these units. There is also 17% increase in meta-volcanic block. No change in accuracy of Yoğurtdağı member and Söğütlü conglomerate is observed. In general, improvement in classification is observed upon integration of DEM layer to the classification and overall accuracy was increased by more than 3%.

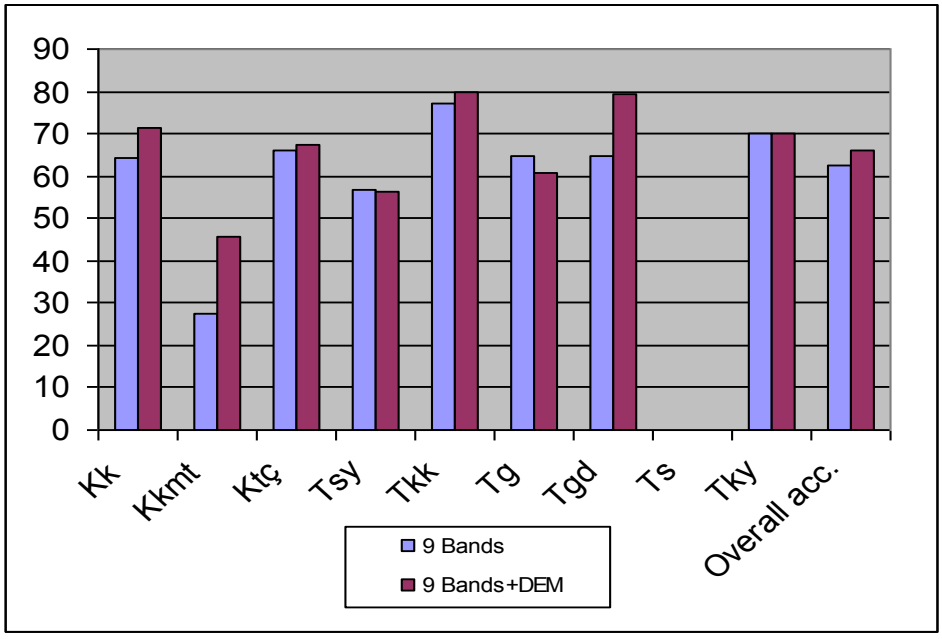

Figure 4. 14: Classification accuracy for each class using nine ASTER bands and DEM (Kk: Kömür Mb., Kkmt: Meta-volcanic block, Ktç: Çerpaçin Mb., Tsy: Yağbasan Mb., Tkk: Refahiye Oph. Complex, Tg: Gülandere Fm., Tgd: Dištaş Agglomerate, Ts: Söğütlü Conglomerate, Tky: Yoğurtdağı Mb.)

4.2.3.2 Slope

The slope (Figure 4.15) ranges between 0 and 72 degrees. The steepest slopes are observed mostly in Kömür member and partly in Gülandere formation.

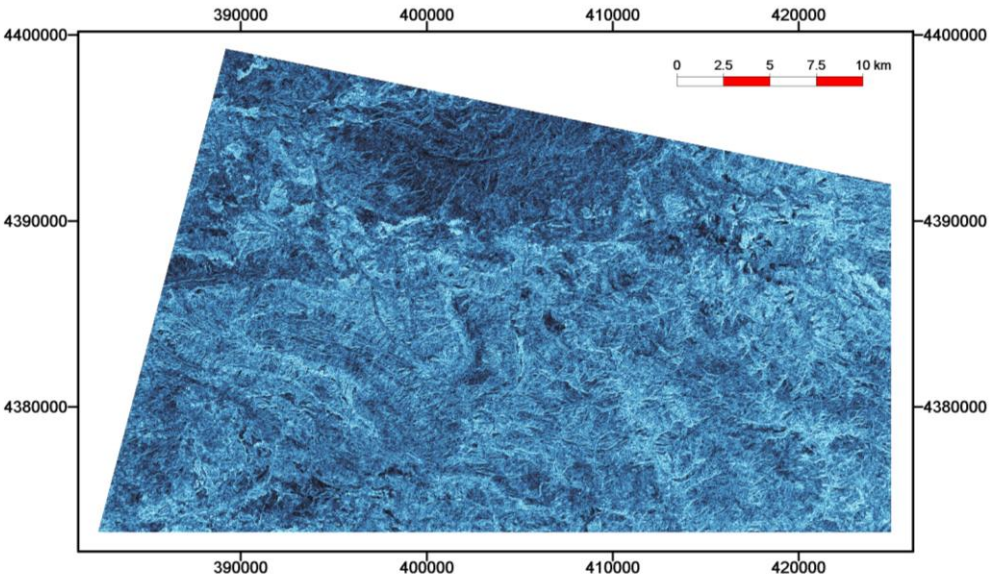

Figure 4. 15: Slope map of study area, dark colors show steeper areas.

Value ranges and mean values of slope for each formation is given in Figure 4.16. Steepest slopes are observed in Çerpaçin member and lowest in Kömür member.

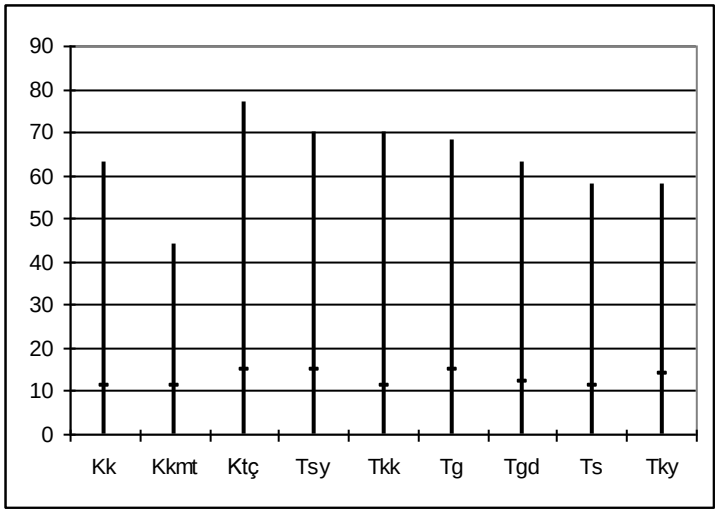

Figure 4. 16: Slope value ranges for each formation.

The classified image using slope and nine ASTER bands as input is given in Figure 4.17 and the error matrix in Table 4.8.

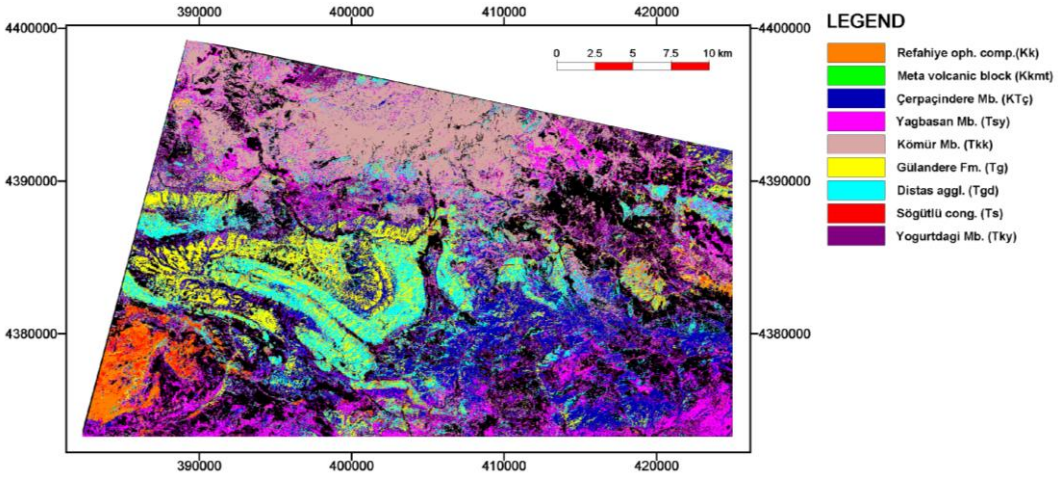

Figure 4. 17: Result of classification with nine ASTER bands together with slope

Table 4. 8: Error matrix of classification with nine ASTER bands and Slope

ES / TS	Kk	Kkmt	Ktç	Tsy	Tkk	Tg	Tgd	Ts	Tky	Total	Acc. (%)
Kk	9	4	0	2	0	0	0	7	0	22	40,91
Kkmt	0	4	0	0	0	0	0	0	0	4	100
Ktç	2	0	52	8	1	7	0	0	1	71	73,24
Tsy	0	0	4	33	6	0	0	1	3	47	70,21
Tkk	0	0	19	14	65	5	0	0	5	108	60,19
Tg	0	0	3	0	0	33	9	0	0	45	73,33
Tgd	2	3	1	1	2	6	25	1	0	41	60,98
Ts	10	0	1	0	0	0	0	3	0	14	71,43
Tky	5	0	0	4	0	0	0	0	11	20	55,00
Total	28	11	80	62	74	51	34	12	20	372	
Acc(%)	67,86	36,36	65,0	53,23	87,84	64,71	73,53	0	55		
Overall Acc(%)	65,05										

As seen from the plot (Figure 4.18), there is 4% increase in the accuracy of Kömür member and also 9% improvement in the Dıştaş agglomerate, similar to the result of classification with DEM. In addition, Refahiye Ophiolitic complex and meta-volcanic block classes show improved accuracies in this case compared to the initial nine band classification. No change in accuracy is observed for Söğütlü conglomerate and Gülandere member and 15% decrease in Yoğurtdağı member is observed. Combination of slope layer together with the nine ASTER bands resulted in an improvement of 3% in the overall accuracy.

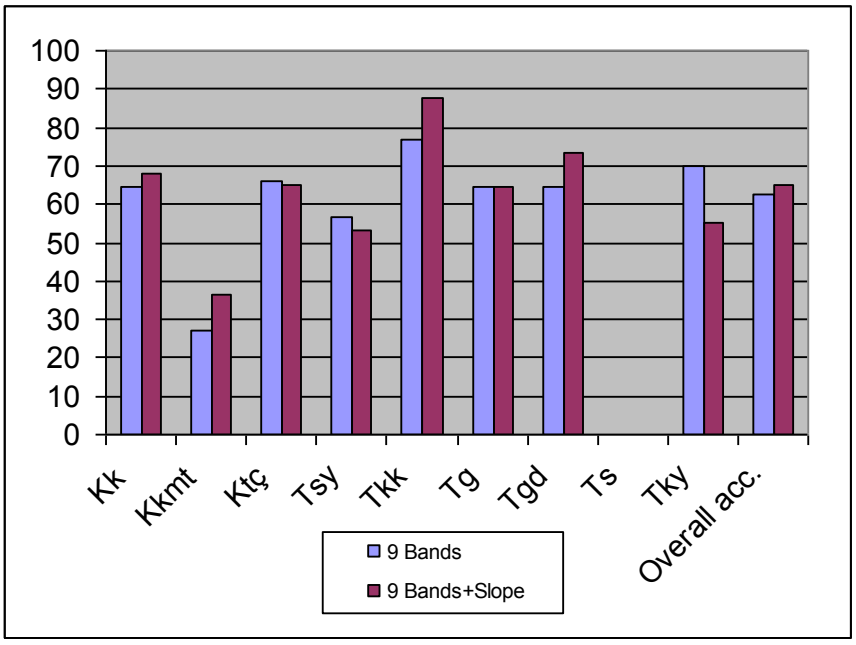

Figure 4. 18: Classification accuracy for each class using nine ASTER bands and slope (Kk: Kömür Mb., Kkmt: Meta-volcanic block, Ktç: Çerpaçin Mb., Tsy: Yağbasan Mb., Tkk: Refahiye Oph. Complex, Tg: Gülandere Fm., Tgd: Dıştaş Agglomerate, Ts: Söğütlü Conglomerate, Tky: Yoğurtdağı Mb.)

4.2.3.3 Profile Curvature

The SML (Spatial Manipulation Language) script computes both curvatures in one pass through the elevation raster (DEM). Because most DEMs include errors and processing artifacts (such as terracing on slopes) that can affect the curvature computation, the script provides the option of applying an initial smoothing filter to the elevation values, and the choice of filter size. The curvature values are computed from a local best-fit mathematical surface for each cell neighborhood, a procedure that provides some additional smoothing (TNT User Manual).

The script allows choose the curvature unit to be chosen; i.e radians per meter or radians per hundred meters. The values for profile curvature change between -0.02 and 0.03, from concave up to convex up respectively and the result raster is provided as 32bit. However, in order to be put as an input, it was rescaled to 8bit (Figure 4.19). The value ranges for profile curvature is given in Figure 4.20.

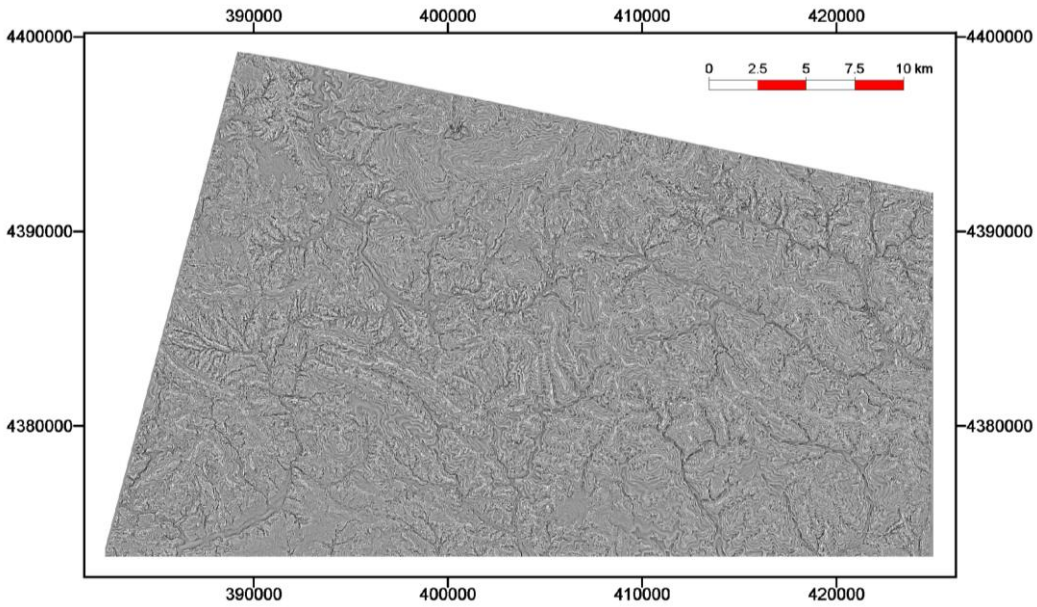

Figure 4. 19: Profile curvature raster of the study area

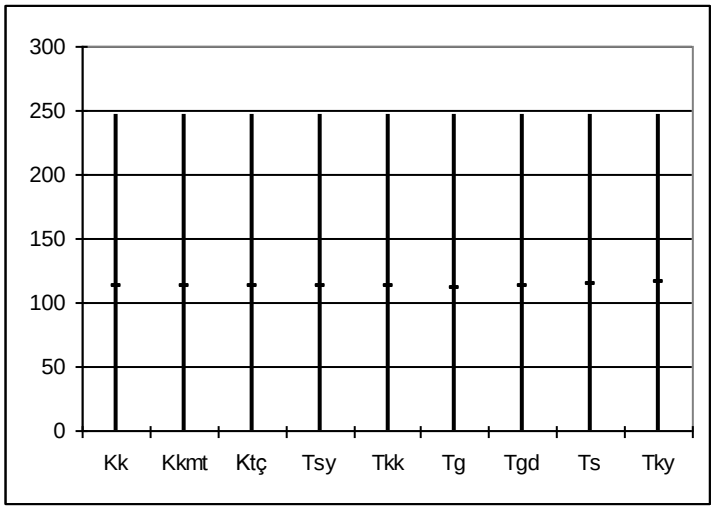

Figure 4. 20: Profile curvature value ranges for each formation.

The classified image is given in Figure 4.21 and the error matrix in Table 4.9. Visual comparison with the reference geological map shows that there is an increase in misclassified pixels especially in Yağbasan Member and Dištaş agglomerate.

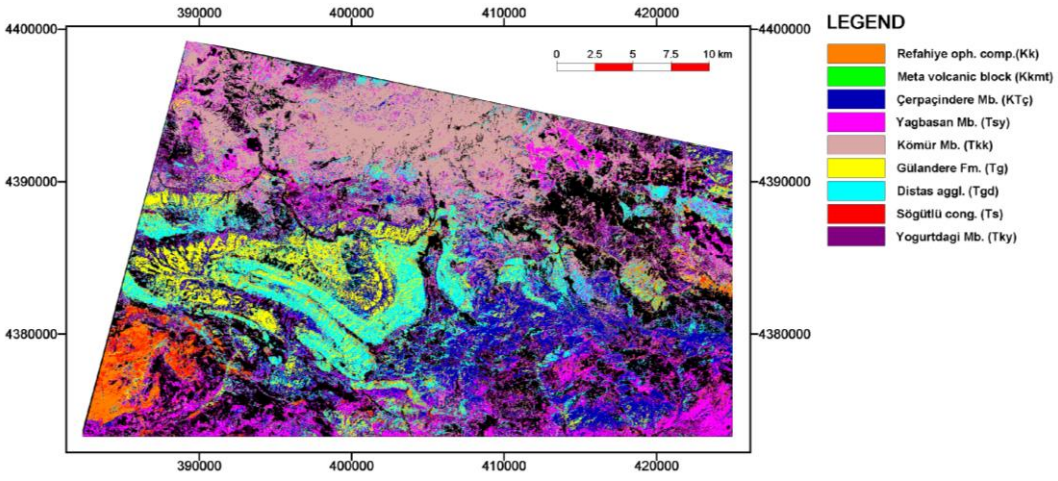

Figure 4.21: Result of classification with nine ASTER bands together with profile curvature

Table 4. 9: Error matrix of classification with nine ASTER bands and profile curvature

ES / TS	Kk	Kkmt	Ktç	Tsy	Tkk	Tg	Tgd	Ts	Tky	Total	Acc. (%)
Kk	9	5	0	2	0	0	0	8	0	24	37,50
Kkmt	0	2	0	0	0	0	0	0	0	2	100
Ktç	2	0	52	7	1	7	0	0	2	71	73,24
Tsy	0	0	2	30	11	0	0	1	2	46	65,22
Tkk	0	0	20	18	56	4	0	0	3	101	55,45
Tg	1	0	55	0	0	32	12	0	0	50	64,0
Tgd	2	3	1	0	3	7	22	0	0	38	57,89
Ts	10	0	0	0	0	0	0	3	0	13	76,92
Tky	4	1	0	5	3	1	0	0	13	27	48,15
Total	28	11	80	62	74	51	34	12	20	372	
Acc(%)	67,86	18,18	65,0	48,39	75,68	62,75	64,71	0	65		
Overall Acc(%)	60,75										

Assessment made from the visual interpretation is also evident in the overall accuracy and also accuracy of each class (Figure 4.22). The overall accuracy for this case is given as 60.75% and shows decrease in comparison to the initial nine band classification result, upon contribution of profile curvature parameter. The value ranges for this parameter for all classes cover the same interval and the mean values of each class are similar, which can be attributed to the decrease in accuracy.

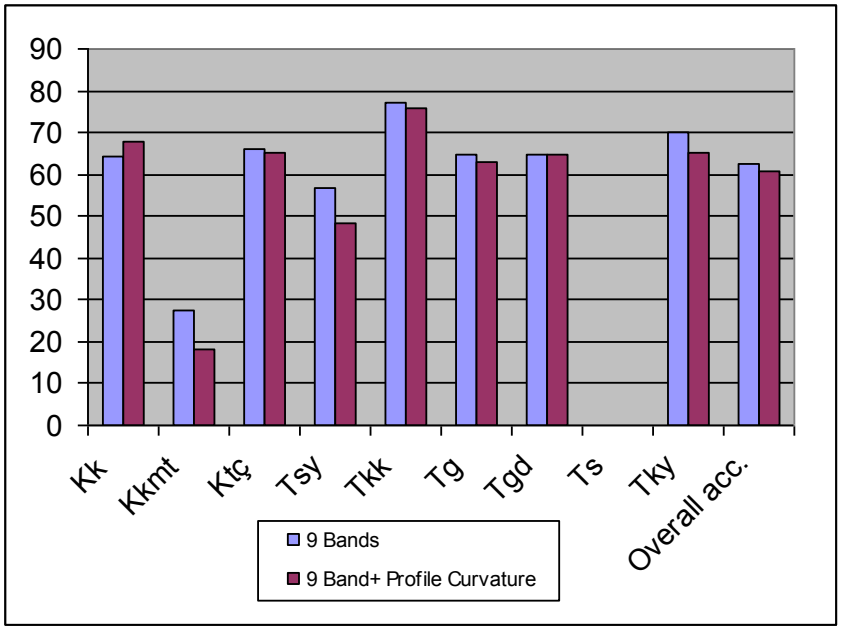

Figure 4.22: Classification accuracy for each class using nine ASTER bands and profile curvature (**Kk:** Kömür Mb., **Kkmt:** Meta-volcanic block, **Ktç:** Çerpaçin Mb., **Tsy:** Yağbasan Mb., **Tkk:** Refahiye Oph. Complex, **Tg:** Gülandere Fm., **Tgd:** Dişţaş Agglomerate, **Ts:** Söğütlü Conglomerate, **Tky:** Yoğurtdağı Mb.)

4.2.3.4 Plan Curvature

Plan curvature is derived in the same way as profile curvature. The plan curvature raster computed from the SML script gives values between -0.04 and 0.06, positive values indicating convex outward surfaces. The result raster is provided as 32bit. However, in order to be put as an input, it was rescaled to 8bit. Plan curvature raster derived from DEM is given in Figure 4.23 and value ranges in Figure 4.24.

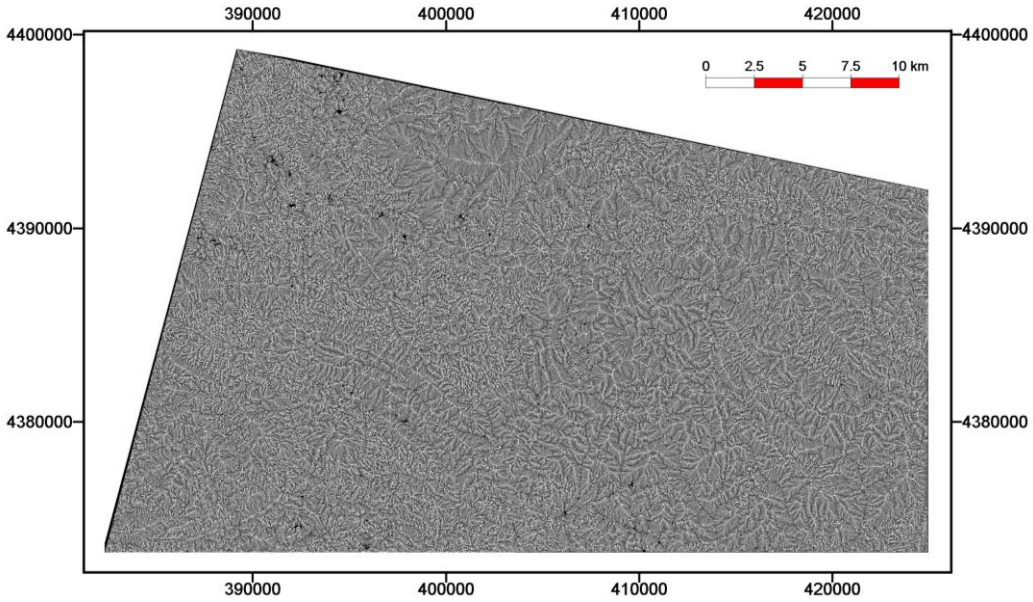

Figure 4. 23: Plan curvature raster of the study area

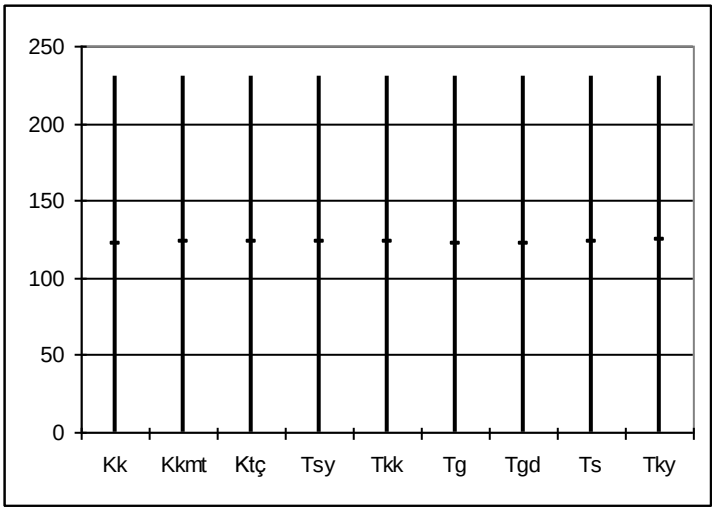

Figure 4. 24: Plan curvature value ranges for each formation.

The classified image using nine ASTER bands and plan curvature as input is given in Figure 4.25 and the error matrix in Table 4.10.

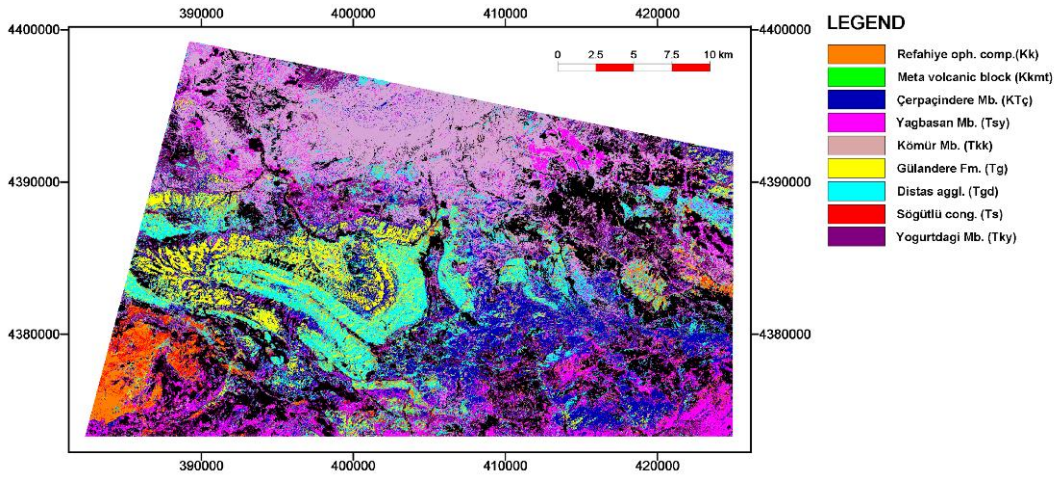

Figure 4. 25: Result of classification with nine ASTER bands together with plan curvature

Table 4. 10: Error matrix of classification with nine ASTER bands and plan curvature

ES / TS	Kk	Kkmt	Ktç	Tsy	Tkk	Tg	Tgd	Ts	Tky	Total	Acc. (%)
Kk	9	6	0	2	0	0	0	7	0	24	37,50
Kkmt	2	1	0	0	0	0	0	0	0	3	66,67
Ktç	2	0	53	6	0	5	0	0	1	67	79,10
Tsy	0	0	2	30	7	0	0	1	3	43	69,77
Tkk	0	0	20	19	59	4	0	0	3	105	56,19
Tg	1	0	4	1	0	36	13	0	0	55	65,45
Tgd	0	1	1	1	3	6	21	0	0	33	63,64
Ts	9	0	0	0	0	0	0	4	0	13	69,23
Tky	5	3	0	3	5	0	0	0	13	29	44,83
Total	28	11	80	62	74	51	34	12	20	372	
Acc(%)	71,43	0	66,25	48,39	79,73	70,59	61,76	0	65		
Overall Acc(%)	62,37										

Among all the units the most significant changes are 6% increase in Refahiye Ophiolitic complex unit and 3% in Kömür Member. The accuracy of meta-volcanic block is decreased to 0%. As a result of the similarity between the plan curvature values given in Figure 4.24, generally the accuracies of all the units showed more or less same values as in the initial classification (Figure 4.26).

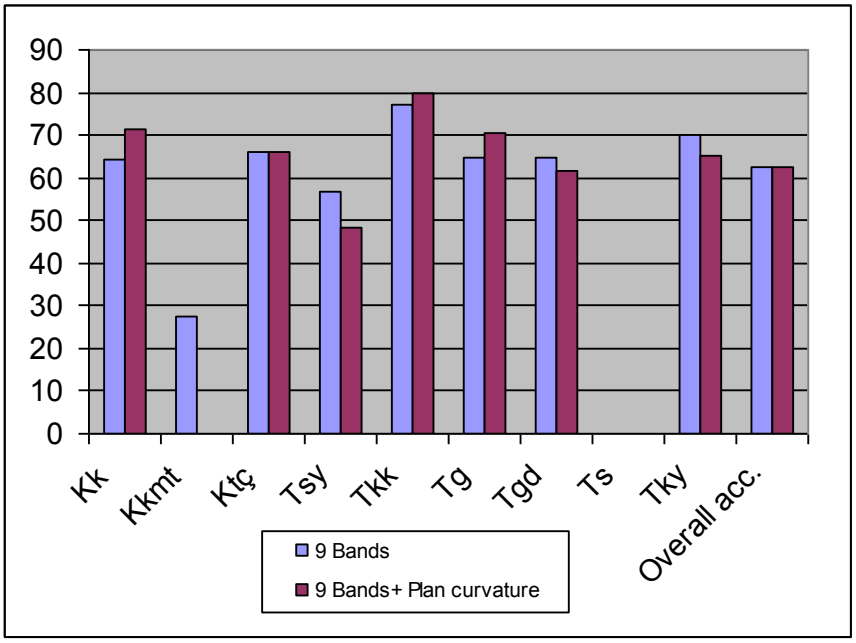

Figure 4. 26: Classification accuracy for each class using nine ASTER bands and plan curvature (Kk: Kömür Mb., Kkmt: Meta-volcanic block, Ktç: Çerpaçin Mb., Tsy: Yağbasan Mb., Tkk: Refahiye Oph. Complex, Tg: Gülandere Fm., Tgd: Dişta Agglomerate, Ts: Söğütlü Conglomerate, Tky: Yoğurtdağı Mb.)

4.2.3.5 Drainage network density

The present day river network reflects the distribution of erodibilities. The differences in erodibility of lithologies clearly influence the shape of drainage patterns. Rivers seem to prefer incision into highly erodible rocks (Kühni and Pfiffner, 2001).

DEM can be used for watershed analysis and several hydrologic properties such as basins and drainage patterns can be extracted and studied. Calculation of drainage density using and SML script resulted in the following image (Figure 4.27). In the image white areas show high density and dark areas are low density. The value ranges are given in Figure 4.28.

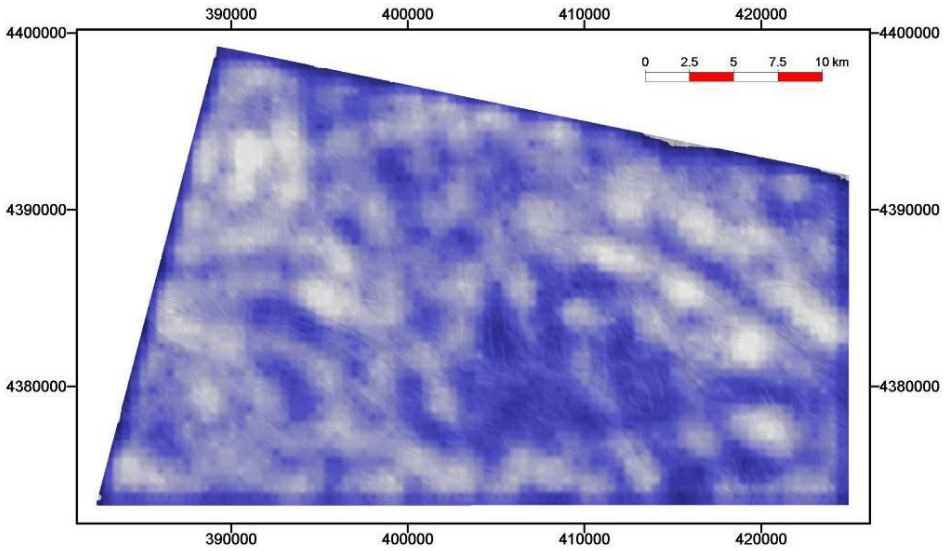

Figure 4. 27: Drainage density of the study area

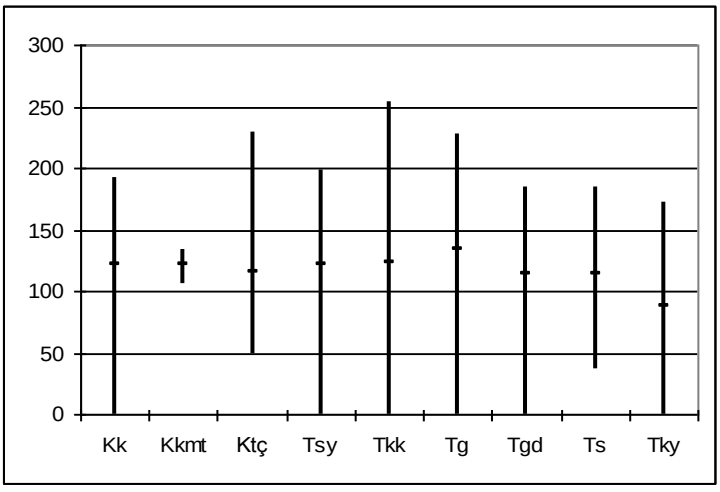

Figure 4. 28: Drainage density value ranges for each formation.

The classified image using drainage density raster and nine ASTER bands is given in Figure 4.29 and error matrix in Table 4.11. It can be said that the classification result displays well match with the reference map for Dištaş agglomerate among all other classification trials.

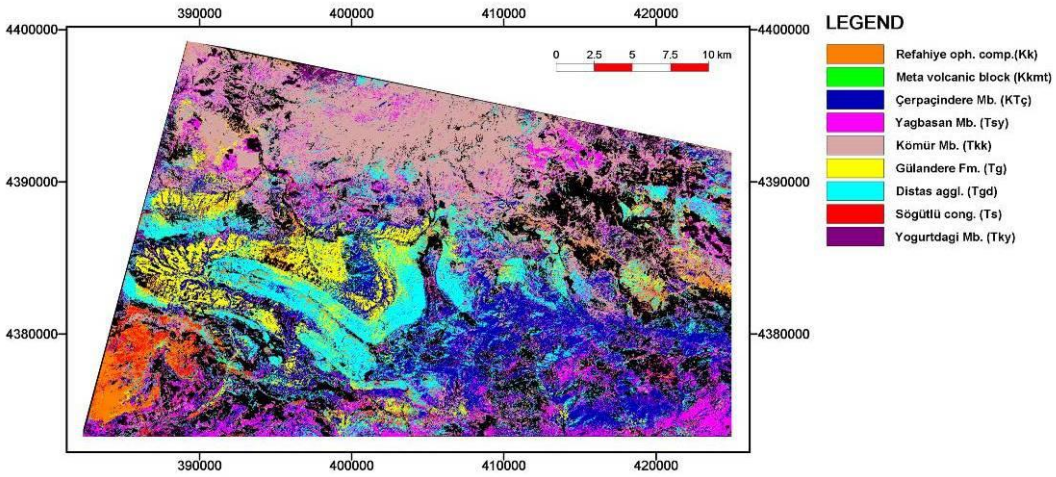

Figure 4. 29: Result of classification with nine ASTER bands and drainage density

Table 4. 11: Error matrix of classification with nine ASTER bands and drainage density

ES / TS	Kk	Kkmt	Ktç	Tsy	Tkk	Tg	Tgd	Ts	Tky	Total	Acc. (%)
Kk	7	4	1	0	0	0	0	5	0	17	41,18
Kkmt	0	3	0	0	0	0	0	0	0	3	100
Ktç	2	0	52	9	0	7	0	0	1	71	73,24
Tsy	0	0	2	35	10	2	1	0	3	53	66,04
Tkk	4	0	21	15	60	3	0	0	2	105	57,14
Tg	1	0	4	0	0	34	2	0	0	41	82,93
Tgd	2	4	0	2	4	5	31	2	0	50	62,00
Ts	12	0	0	0	0	0	0	5	0	17	70,59
Tky	0	0	0	1	0	0	0	0	14	15	93,33
Total	28	11	80	62	74	51	34	12	20	372	
Acc(%)	67,86	27,27	65	56,45	81,08	66,67	91,18	0	70		
Overall Acc(%)	66,67										

In addition, increases in accuracy for Kömür member and Refahiye Ophiolitic complex are observed (Figure 4.30). The overall accuracy was increased to 66,67% from 62,37%, which is the largest increase among all ancillary data classifications.

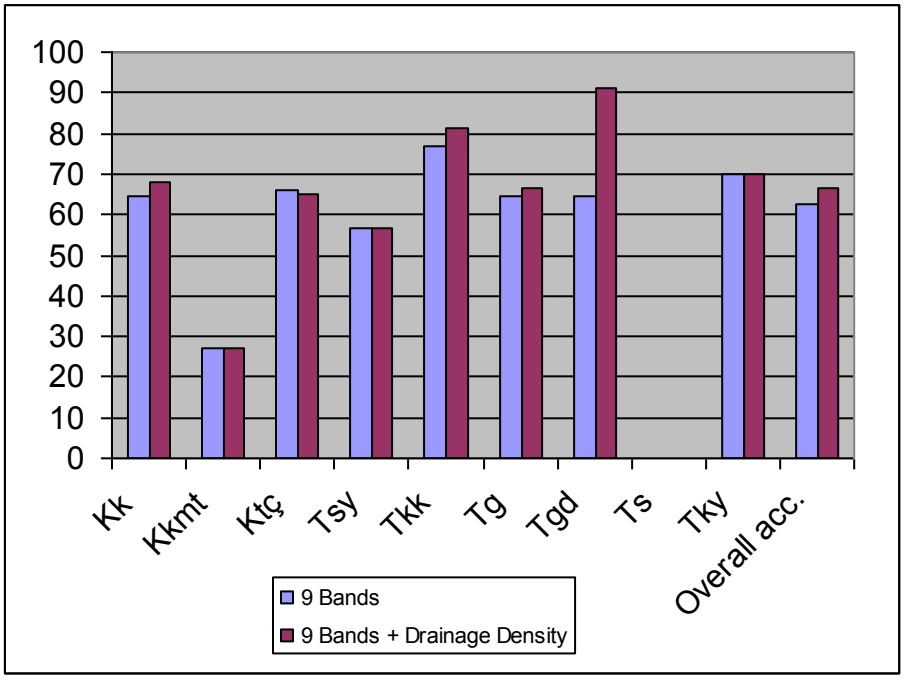

Figure 4. 30: Classification accuracy for each class using nine ASTER bands and drainage density (Kk: Kömür Mb., Kkmt: Meta-volcanic block, Ktç: Çerpaçin Mb., Tsy: Yağbasan Mb., Tkk: Refahiye Oph. Complex, Tg: Gülandere Fm., Tgd: Dişţaş Agglomerate, Ts: Söğütlü Conglomerate, Tky: Yoğurtdağı Mb.)

4.2.3.6 All Terrain Parameters

Result of classification using all terrain parameters all at once in addition to nine ASTER bands is given in Figure 4.31. Error matrix for this classification is provided in Table 4.12. Visual comparison with the reference map reveals that there is a good correlation for the most of the units than any other classification.

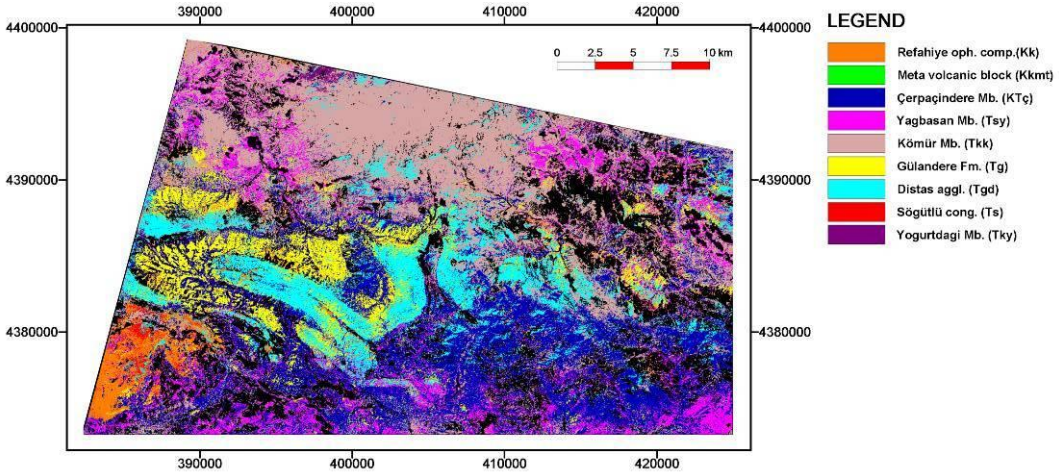

Figure 4. 31: Result of classification with nine ASTER bands together with all five ancillary data layers

Table 4. 12: Error matrix of classification with nine ASTER bands and all ancillary data

ES / TS	Kk	Kkmt	Ktç	Tsy	Tkk	Tg	Tgd	Ts	Tky	Total	Acc. (%)
Kk	9	2	0	0	0	0	0	6	0	17	52,94
Kkmt	0	0	0	0	0	0	0	0	0	0	0
Ktç	4	1	52	7	2	10	0	0	1	77	67,53
Tsy	0	08	2	33	5	1	0	0	3	50	66
Tkk	3	0	26	21	64	4	0	0	1	119	53,78
Tg	1	0	0	1	0	31	2	0	0	35	88,57
Tgd	0	0	2	0	3	5	32	2	0	44	72,73
Ts	11	0	0	0	0	0	0	4	0	15	73,33
Tky	0	0	0	0	0	0	0	0	15	15	100
Total	28	11	80	62	74	51	34	12	20	372	
Acc(%)	71,43	0	65	53,23	86,49	60,78	94,12	0	75		
Overall Acc(%)	66,44										

The overall accuracy was increased from 62,37% to 66,44% upon integration of all ancillary data together. Also from the graph given in Figure 4.32, a major increase in accuracy of Dıştaş agglomerate and also in Kömür member, Yoğurtdağı member and Refahiye ophiolitic complex is observed.

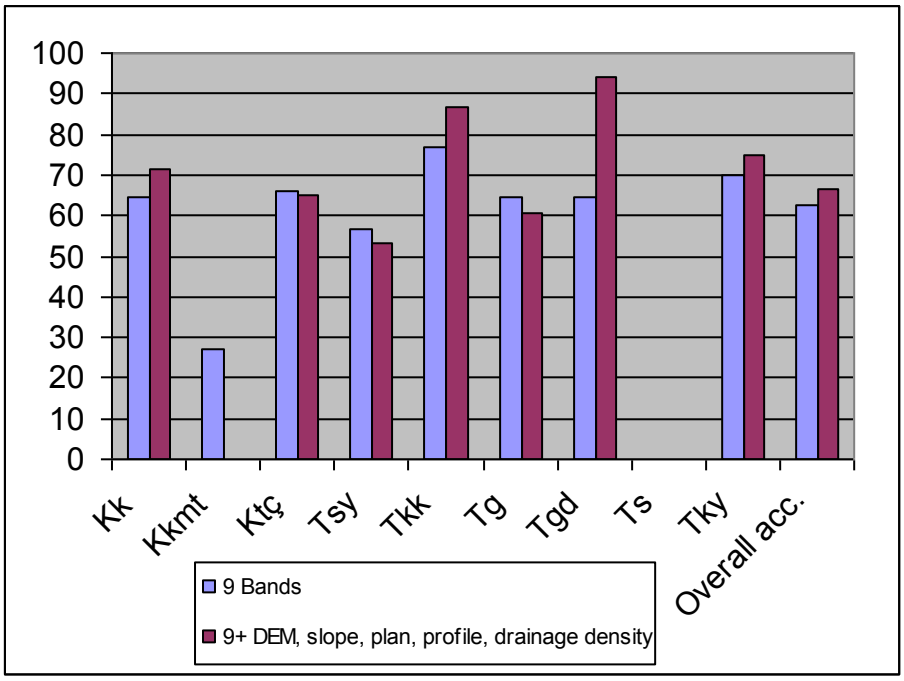

Figure 4. 32: Classification accuracy for each class using nine ASTER bands and the five ancillary data layers (Kk: Kömür Mb., Kkmt: Meta-volcanic block, Ktç: Çerpaçin Mb., Tsy: Yağbasan Mb., Tkk: Refahiye Oph. Complex, Tg: Gülandere Fm., Tgd: Dişţaş Agglomerate, Ts: Söğütlü Conglomerate, Tky: Yoğurtdağı Mb.)

CHAPTER 5

RESULTS AND DISCUSSION

Observing the differences between targets and their backgrounds involves comparing different targets based on any, or all, of the visual elements of tone, shape, size, pattern, texture, shadow, and association (Ouattara et al, 2004).

The purpose of this study was to test whether integration of terrain parameters can aid in improving the mapping accuracy of spectrally similar units. determine which terrain attributes obtained from DEM can be used in extraction of geologic information and which lithologies can be better differentiated on basis of terrain parameters

In the study supervised classification was employed to map the lithological units. Next, with the derived terrain parameters, a method for improving the classification made solely on spectral characteristics was utilized. The methodology involves integrating the surface properties of the classified geological units in addition to the spectral reflectances. The results revealed that integrating topographical parameters aid in improvement of classification where spectral information is not sufficient to discriminate between classes of interest.

In this study, ASTER sensor images were used for interpretation. SWIR and VNIR region bands were utilized as input bands in classification of geological units whereas; TIR region bands were proved to be useful in mapping gypsum units.

Seven different classification trials were conducted : 1. MLC using only nine ASTER bands, 2. MLC using ASTER bands and DEM, 3. MLC using ASTER bands and slope, 4. MLC using ASTER bands and plan curvature, 5. MLC using ASTER bands and profile curvature, 6. MLC using ASTER bands and drainage density and finally 7. MLC using ASTER bands and all ancillary data.

5.1 Principal Components Analysis of Ancillary Data Layers

In order to examine whether there are similar information contained in the ancillary data bands Principal Component Analysis (PCA) is utilized.

PCA is a way of identifying patterns and correlation, if any, in a dataset. This process seeks to maximize (statistically) the amount of information (or variance) from the original data into the least number of new components and enables expressing the data in order to emphasize their similarities and differences. Having said this, PCA of the ancillary data was carried out and results of the analysis are given in Table 5.1.

Eigenvector statistics in each PC identifies the PC image in which the information is contained. This information represents a small fraction of the total information contained in the original ancillary data; however it is supposed that loaded information relates to the attribute of the required class.

Table 5.1: Correlation between Input Rasters and PC, and associated eigenvalue percentages

Axis	Slope	DEM	Profile	Plan	Drainage Density	Eigenvalues (%)
1	0,153	-0,979	-0,202	-0,080	0,311	42,10
2	-0,001	0,138	-0,976	-0,206	-0,063	28,94
3	0,056	-0,149	0,012	0,005	-0,948	18,73
4	-0,043	-0,007	-0,058	0,975	0,003	7,65
5	0,986	0,010	0,001	0,015	0,005	2,58

PC1 explained less than half of the variation in the entire dataset and the second PC explained 28,94% of the variation in the dataset. Moreover, from the percentages and improvement in the overall classification involving the abundant parameter in the fifth component; slope, information in the higher-level component is still useful for the classification.

In order to detect the contribution of each parameter to each PC axis, component loadings are analyzed. It can be interpreted that PC1 is highly negatively related to the abundance of DEM and weakly negatively related to abundance of profile curvature and positively to drainage density and slope. On the other hand, PC2 is negatively related to profile curvature. PC3 reflects that drainage density is negatively loaded in this axis. Plan curvature is the abundant parameter in PC4 and slope in PC5.

It is evident that the information contained in each band is dissimilar with eachother though the magnitude of information carried by each vector loadings could be small but vital. Therefore each band holds different information and it is appropriate to evaluate each ancillary band as a separate data source and not eliminate in the integration procedure.

In addition to gypsum units denoted in the geological map, some regions showing gypsum anomalies are noticed from the sulfate index image. These areas are in the Kömür member, however they might be the continuum of Hafik or Yağbasan gypsum located in close vicinity to these (Figure 5.1). It is possible that these gypsum which are not shown in the published 1/100 000 scale geological map might be missed out or might be an error arising from the sulfate index methodology. Further studies can be conducted to test the effectiveness of gypsum mapping in the region.

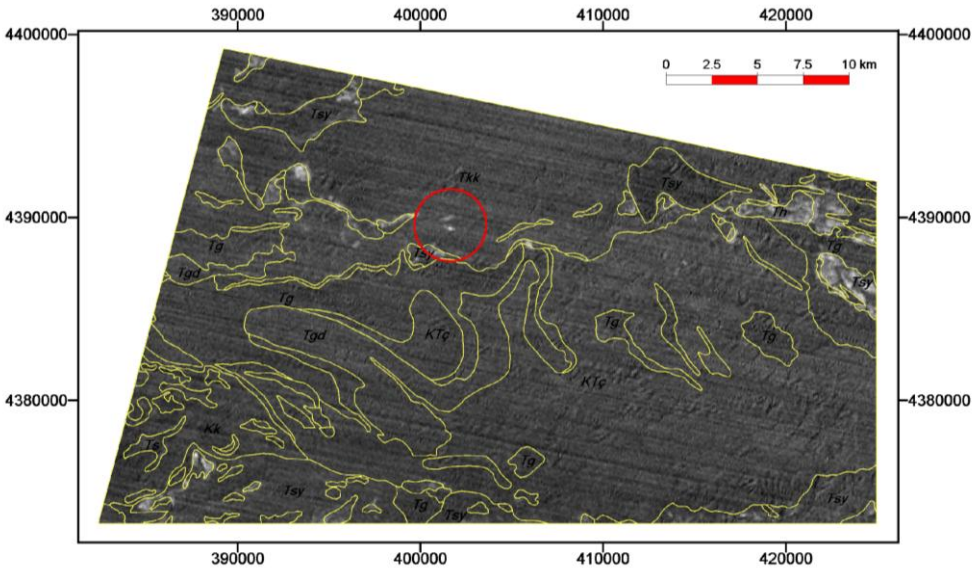

Figure 5. 1: Sulfate index image showing new gypsum units in red circled area

Error matrix for the best classification is modified by adding in the accuracy for Hafik Formation, consisting of gypsum. The 100% accuracy from this unit results in an increase of 2.5% in the overall accuracy and accuracy rises up to 69,15%. This can be evaluated as a post-classification sorting and resluts show that upon addition of a classified monomineralic unit to the classification result, acccuracy is increased.

Table 5. 2: Resultant error matrix of classification with nine ASTER bands and drainage density after insertion of gypsum class

ES / TS	Kk	Kkmt	Ktç	Tsy	Tkk	Tg	Tgd	Ts	Tky	*Th*	Total	Acc. (%)
Kk	7	4	1	0	0	0	0	5	0	***0***	17	41,18
Kkmt	0	3	0	0	0	0	0	0	0	***0***	3	100
Ktç	2	0	52	9	0	7	0	0	1	***0***	71	73,24
Tsy	0	0	2	35	10	2	1	0	3	***0***	53	66,04
Tkk	4	0	21	15	60	3	0	0	2	***0***	105	57,14
Tg	1	0	4	0	0	34	2	0	0	***0***	41	82,93
Tgd	2	4	0	2	4	5	31	2	0	***0***	50	62,00
Ts	12	0	0	0	0	0	0	5	0	***0***	17	70,59
Tky	0	0	0	1	0	0	0	0	14	***0***	15	93,33
Th	***0***	***0***	***0***	***0***	***0***	***0***	***0***	***0***	***0***	***30***	***30***	***100***
Total	28	11	80	62	74	51	34	12	20	***30***	402	
Acc(%)	67,86	27,27	65	56,45	81,08	66,67	91,18	0	70	***100***		
Overall Acc(%)	69,15											

In selection of classes, while taking training areas for each class from formation polygons, it was assumed that a unit named as “formation” or “member” had more or less homogeneous lithic characteristics, in other words arising from the concept or definition of Formation; i.e “formations can be defined on the basis of a single lithic type, repetitions of two or more lithic types, or extreme lithic heterogeneity, where such heterogeneity constitutes a form of unity when compared to adjacent units.” (Boggs, 2001)

Classification and accuracy was limited by the use of only one training set. In addition, scale and therefore the detail level of the geological map used in this study was a constraint in selection of classes. In spite the spectral similarity of most geological materials within the area, spectral resolution of ASTER sensor might have provided more lithological boundaries to be distinguished, if not all. If class selection were done from 1/25 000 scale geological map rather than a coarser 1/100 000 map there might have been more classes that can be discriminated.

The classification accuracy for Kömür member is higher comparatively to the other units in all combinations of input bands used in the classification. The Söğütlü conglomerate showed very low classification accuracy in all image variables.

Plan and profile curvature data were found to be not useful as the other three; namely DEM, slope and drainage density. The resolution of the DEM from which these data were created is considered to be important.

CHAPTER 6

CONCLUSION

Remote sensing and integration of available ancillary data using image classification as applied in this study, was found to be useful in mapping less spectrally separable geological units having similar rock compositions. Accuracy of the classification was increased by 4% using all available ancillary data. Moreover, more than 10% increase in accuracies of individual classes is observed as a result of integrating ancillary data to the classification procedure. However, the largest increase in accuracy is observed when drainage density layer is utilized and upon addition of the extracted gypsum class, the accuracy is increased from the initial 62, 37% up to 69,15%. At this point, the value ranges covered by each formation for each ancillary data layer comes into question. The variation between the value ranges for classification units affects the success of integration of an ancillary layer into the classification for increasing the accuracy.

Results are compared with the existing geological information to show the effectiveness of the method for achieving lower cost and higher accuracy in geological mapping of units with similar spectral characteristics. Geological mapping will surely always necessitate field work. However, mapping procedure can be greatly eased through the use of image interpretation, especially if large areas are to be mapped.

The end results presented in this study are not meant to be used for systematic purposes. This was an exploratory study to determine the effect of integration of

available terrain attributes on classification results and examine the relationships between terrain parameters and lithologies in the study area selected. Conducting further studies is necessary in order to use this method for detailed studies.

Ground truth verification should be done for the area using ground control points and results of interpretation and analysis should be checked in the field both for the lithological classification and terrain parameters. In addition as a further research topic, classification of morphotectonic parameters may be considered. Examination of further means of fusion of ancillary data and spectral data together with more thorough evaluation of terrain attributes may help to improve results found in this study.

REFERENCES

Aktimur, H. T., 1988, 1/100 000 Ölçekli Açınsama Nitelikli Türkiye Jeoloji Haritaları Serisi Divriği F26 Paftası, MTA, Ankara, 11 pg.

Aktimur, H. T., Tütüncü, K., 1988, 1/100 000 Ölçekli Açınsama Nitelikli Türkiye Jeoloji Haritaları Serisi Divriği-F25 Paftası, MTA, Ankara, 11 pg.

Aktimur, H. T., Tekirli, M. E., Yurdakul, M.E., 1990, Geology of the Sivas Erzincan Tertiary Basin, MTA Bulletin, 111. 21-30.

Altunsoy, M., Özçelik, O., 1998, Organic facies characteristics of the Sivas Tertiary Basin Turkey, Journal of Petroleum Science and Engineering, 20, 73–85.

Arpat, E., 1964, Gürlevik dağı bölgesinin ve kuzeyinin genel jeolojisi ve petrol imkanları. MTA Raporu No. 4180, (yayınlanmamış), Ankara.

Artan, Ü., ve Sestini, G., 1971, Sivas-Zara-Beypınan bölgesinin jeolojisi: MTA Derg., 76, 80-97.

Baldridge, A.M., Hook, S.J., Grove, C.J. and Rivera, G., 2009, The Aster Spectral Library version 2.0, Remote Sensing of Environment, 113, 711-715.

Boggs Jr, S. 2001, Principles of Sedimentology and Stratigraphy, 3rd Edition, New Jersey, Prentice Hall, 726 pg.

Brown, D. G., Lusch, D.P., Kenneth, A.D, 1998, Supervised classification of types of glaciated landscapes using digital elevation data, Geomorphology, 21, 233-250.

Burbank, D.W., Anderson, R.S., 2001, Tectonic geomorphology,1st Ed., Blackwell Science, Malden, Mass., 274 pg.

Cater, J.M.L., Hanna, S.S., Ries, A.C., Turner, P., 1991. Tertiary evolution of the Sivas basin, Central Turkey, Tectonophysics, 195, 29-46.

Drury, S.A., 2001. Image Interpretation in Geology, 3rd Ed., Blackwell Science, 290 pg.

Evans, D., 1988, Multisensor classification of sedimentary rocks, Remote Sensing of Environment. Vol. 25, pp. 129-144.

Frohn, R. C., 2006 The use of landscape pattern metrics in remote sensing image classification, International Journal of Remote Sensing, Vol. 27, No. 10, 2025–2032.

Fujisada, H., 1995, Design and performance of ASTER instrument, Proceedings of SPIE, the International Society for Optical Engineering, 2583, 16– 25.

Gad, S. and Kusky, T., 2007, ASTER spectral ratioing for lithological mapping in the Arabian–Nubian shield, the Neoproterozoic Wadi Kid area, Sinai, Egypt, Gondwana Research, 11, 326–335.

Grohmann, C.H., Riccomini C., and Alves F.M., 2007, SRTM-based morphotectonic analysis of the Pocos de Caldas Alkaline Massif, southeastern Brazil, Computers & Geosciences, 33, 10–19.

Gürsoy, H., Piper, J.D.A., Tatar O., Temiz H., 1997, A palaeomagnetic study of the Sivas Basin, central Turkey: Crustal deformation during lateral extrusion of the Anatolian Block, Tectonophysics, 271, 89-105.

Hengl, T.,Gruber, S. and Shrestha, D., 2003, Digital Terrain Analysis in ILWIS, Lectures notes and user guide, International Institute for Geo-Information Science and Earth Obsevation, Enschede, 56 pg.

http://asterweb.jpl.nasa.gov/content/05_bibliography/03_Workshop/presentations/rad-cal-biggar.ppt#31 visited on January 2009.

http://atlas.cc.itu.edu.tr/~okay/AralOkayPapersThematically.htm visited on February 2009.

http://asterweb.jpl.nasa.gov/swir-alert.asp visited on March 2009.

Hutchinson, C.F.1982, techniques for Combining Landsat and Ancillary Data for digital Classification Improvement, Photogrammetric Engineering and Remote Sensing, Vol 48, No:1, 123-130.

Jordan, G., Meijninger, B.M.L., Van Hinsbergen D.J.J., Meulenkamp, J.E., Van Dijk, P.M.,2005, Extraction of morphotectonic features from DEMs: Development and applications for study areas in Hungary and NW Greece, International Journal of Applied Earth Observation and Geoinformation, 7, 163–182.

Kam, T. S., 1995, Integrating GIS and remote sensing techniques for urban land-cover and land-use analysis, Geocarto International, 10, 39–49.

Kerle, N., Janssen, L.F.F., Huurneman G., 2004, Principles of Remote Sensing (ITC Educational Textbook series), 3rd Edition, 250 pg.

Koşun, E., Çiner, A., Zara güneyi (sivas havzasi) karasal-sığ denizel miyosen çökellerinin litostratigrafisi ve fasiyes özellikleri, 2002, MTA Dergisi, 125, 65-88.

Kurtman, F., 1961, Sivas-Divriği arasındaki sahanın jeolojisi ve jipsli seri hakkında müşahedeler, MTA Dergisi. no. 56.

Kurtman, F., 1973, Sivas-Hafik-Zara ve İmranlı bölgesinin jeolojik ve tektonik yapısı, MTA Bulletin, 80, 1-32.

Kühni, A., and Pfiffner, O.A., 2001. The relief of the Swiss Alps and adjacent areas and its relation to lithology and structure: topographic analysis from a 250-m DEM, Geomorphology, 41, 285–307.

Lillesand T. M., Kiefer, R. W., Chipman, J.W., 2004, Remote sensing and image interpretation, 5th Edition, New York , Wiley, 763 pg.

Masoud, A., Koike, K., 2006, Tectonic architecture through Landsat-7 ETM+/SRTM DEM-derived lineaments and relationship to the hydrogeologic setting in Siwa Region, NW Egypt, Journal of African Earth Sciences, 45, 467–477.

Microimages TNT-MIPS, 2008. (http://www.microimages.com) visited on December 2008.

Ninomiya, Y., 2002, Mapping quartz, carbonate minerals and mafic-ultramafic rocks using remotely sensed multispectral thermal infrared ASTER data, proceedings of SPIE, vol. 4170, 191-202.

Ocakoğlu, F., 1999, Evidences of Ductile Deformation in Evaporites Around Zara Area (E sivas), sivas basin Mineral Res. Expl. Bul., 121, 19-31.

Ouattara, T., Couture, R., Bobrowsky, P.T., and Moore, A., 2004, Remote Sensing: Theory and Principles, Geological Survey of Canada, Open File 4542, 102 pg.

Öztan, N.S., 2007, Evaporate Mapping in Bala Region (Ankara) by Remote Sensing Techniques, Msc thesis, METU, 89 pg.

Platzman, E.S., Tapirdamaz, C., Sanver, M., 1998, Neogene anticlockwise rotation of central Anatolia (Turkey): preliminary palaeomagnetic and geochronological results, Tectonophysics, 299, 175–189.

Qui F., Abdelsalam M., Thakkar P., 2006. Spectral analysis of ASTER data covering part of the Neoproterozoic Allaqi-Heiani suture, Southern Egypt, Journal of African Earth Sciences, 44, 69–180.

Rowan, L. C., Wetlaufer, P. H., Goetz, A. F. H., Billlingsley, F. C., Stewart, J. H., 1974, Discrimination of rock types and detection of hydrotermally altered areas in south–central Nevada. U.S. Geological Survey Professional Paper, 883, 1 – 35.

Rowan, L.C., Mars, J.C., 2003, Lithologic mapping in the Mountain Pass, California Area Using Advanced Spaceborne Thermal Emission and Reflection Radiometer (ASTER) data, Remote Sensing of Environment, 84(3), 350-366.

Rowan, L.C., Mars, J.C., Simpson, C. J., 2005, Lithologic mapping of the Mordor, NT, Australia ultramafic complex by using the Advanced Spaceborne Thermal Emission and Reflection Radiometer (ASTER), Remote Sensing of Environment 99, 105 – 126.

Sabins, F. F., 1997, Remote sensing : principles and interpretation, 3rd Edition, New York : W.H. Freeman and Co., 494 pg.

Sabins, F. F, 1999, Remote sensing for mineral exploration, Ore Geology Reviews, 14, 157–183.

Strahler, A., 1980, The use of prior probabilities in maximum likelihood classification of remotely sensed data, Remote Sensing of Environment, 10, 1135-1163.

Tso, B., Mather, P.M., 2001, Classification Methods for Remotely Sensed Data, Taylor and Francis Inc, New York, London.

Wilson, J. P., Galant, J. C., 2000, Terrain Analysis: Principles and Applications, Chichester UK & NY, 479 pg.

Yılmaz, A., 1994, Çarpışma Sonrası bir Çanak Örneği: Sivas havzası, Türkiye. Türkiye 10. Petrol Kongresi Bildiriler Kitabı, 21-33.

Yılmaz, A., Yılmaz, H., 2006, Characteristic features and structural evolution of a post collisional basin: The Sivas Basin, Central Anatolia, Turkey, Journal of Asian Earth Sciences, 27, 164–176.